OPTICAL DESIGN OF A COHERENT OPTICAL PROCESSOR

by

William Henry Swantner

A Dissertation Submitted to the Faculty of the

COMMITTEE ON OPTICAL SCIENCES (GRADUATE)

In Partial Fulfillment of the Requirements

For the Degree of

DOCTOR OF PHILOSOPHY

In the Graduate College

THE UNIVERSITY OF ARIZONA

1 9 7 8

THE UNIVERSITY OF ARIZONA

GRADUATE COLLEGE

I hereby recommend that this dissertation prepared under my direction by William Henry Swantner

entitled Optical Design of a Coherent Optical Processor

be accepted as fulfilling the dissertation requirement for the degree of Doctor of Philosophy

James C. Wyant — 12/28/77

Dissertation Director — Date

As members of the Final Examination Committee, we certify that we have read this dissertation and agree that it may be presented for final defense.

Jack D. Gaskill	29 Dec. 1977
Grant R. Stevenson	16 December 1977

Final approval and acceptance of this dissertation is contingent on the candidate's adequate performance and defense thereof at the final oral examination.

STATEMENT BY AUTHOR

This dissertation has been submitted in partial fulfillment of requirements for an advanced degree at The University of Arizona and is deposited in the University Library to be made available to borrowers under rules of the Library.

Brief quotations from this dissertation are allowable without special permission, provided that accurate acknowledgment of source is made. Requests for permission for extended quotation from or reproduction of this manuscript in whole or in part my be granted by the head of the major department or the Dean of the Graduate College when in his judgment the proposed use of the material is in the interests of scholarship. In all other instances, however, permission must be obtained from the author.

SIGNED: William Bwantner

Dedicated to

William E. Mimmack

who introduced me to "the paradise

of mathematicians"

ACKNOWLEDGMENTS

To Ram Sarup for encouraging me to pursue a Ph.D. in optics.

The patience of Robert Shannon and Dick Buchroeder in starting me off in lens design is appreciated.

I am grateful to O. N. Stavroudis and Jack Gaskill for the hours of valuable conversation I've enjoyed with them. My dissertation advisor, James C. Wyant, suggested the single glass problem described in Chapter 4.

Finally, thanks to the numerous friends at McDonnell-Douglas Electronics Co., the Optical Sciences Center, and White Sands Missile Range who charitably listened to my endless talking about this dissertation.

TABLE OF CONTENTS

TABLE OF CONTENTS--Continued

LIST OF ILLUSTRATIONS

LIST OF ILLUSTRATIONS--Continued

LIST OF TABLES

ABSTRACT

This dissertation discusses the design and evaluation of lenses for some coherent optical processing applications. The first order properties are depicted by diagrams of lenses with paraxial ray paths through the system. It is the purpose of this approach to cast the properties of a coherent optical processor in the terms of image forming optics. This will create a compatibility with existing optical design optimization programs. A product of such a formulation is that the lenses can be evaluated with the same program which performed the optimization. Object-pupil relationships are shown. A methodology to treat the diffraction integrals of processors is developed to include an understanding of linear and quadratic phase factors in terms of paraxial optics. In the geometrical optics description of a Fourier Transform Lens (FTL), it is shown that the diffracting object defines the location and the extent of the lens's aperture stop.

The design and the evaluation of several lenses are considered. The usefulness of a doublet telescope objective as an FTL is described with point spread function (psf) calculations. Aberrations are diagnosed from ray fan diagrams. A Vander Lugt matched filter correlator constructed of doublets is then evaluated.

A matched filter correlator constructed from two FTL's of different focal lengths was designed and evaluated. The fabrication data for the lenses and pupil and focal plane locations are stated. Also listed are the data for fabrication of a four element asymmetric FTL.

The design approach and a description of the defect function for minimization of aberrations are given.

A useful concept in coherent processing is the application of multicolor lasers for reasons of photographic emulsion sensitivity, illumination uniformity, and input transparency spatial frequency content. Chromatic correction in the ordinary sense is not required. The impact of this and coding of the optimization program to make effective use of the relaxed requirements are discussed. The final diagrams present data and evaluation of FTL's suitable for use at 632.8 nm and at 488 nm. The scheme to design such lenses using the capability of ACCOS V (ACCOS programs are the copyrighted property of Scientific Calculations, Inc., Rochester, New York) for zoom lens optimization is demonstrated.

CHAPTER 1

INTRODUCTION

The reader is assumed to be familiar with scalar diffraction theory, the Fourier transforming property of lenses, and image formation as presented by Cathey (1974) or Goodman (1968). However, Appendix A, Methods for Studying Optical Processors, develops some methodology for treating the diffraction calculations in a straightforward manner. Use of geometrical optics is made in the treatment, but all the calculations are closely tied to the use of the Fresnel-Kirchoff integral description of the particular situation. It is felt that the consistent use of a single method in treating FTL's and various applications makes for better understanding and appreciation. The integral approach is often abandoned at some point in favor of a less cumbersome method. We show that, when supplemented with some simple geometrical optics principles, the integral treatment remains quite tractable. In both Cathey and Goodman, the pupil functions of the FTL's are assumed to be adequately described by a quadratic phase factor which is independent of spatial frequency. Phase errors in the pupil function (wavefront aberrations) and their dependence on spatial frequency (viz., field angle) are neglected in consideration of more basic concerns.

In this dissertation, we discuss the significance of the psf, characterization of the pupil function in terms of geometrical optics, and the design of lenses for use as FTL's and for use in the Vander Lugt

configuration. The lens design consists in attempts to reduce the wavefront aberrations to a level such that the wavefront converging to any point in the transform plane be spherical. Achievement of this ideal is subject to several constraints. Implementation of the constraints is different for the design of a lens meant only for spatial frequency mapping and for the design of lenses to be used in a Vander Lugt correlator. Ideal linearity of the correlator requires not only that the wavefront for each point in the correlation plane be spherical upon leaving the lens, but that the chief ray for the wavefront be normal to the correlation plane. If the chief ray is not normal to this plane, then the Airy pattern changes with field angle. This last requirement is known to cause difficulties with computation of the transverse ray errors. The exit pupil lies at the image space intersection of the chief ray with the optical axis. If the chief ray is parallel to the axis, the intersection is infinitely distant. Rays traced through the lens, on to the exit pupil, and from there to the rear focal plane lose precision due to limited word length in the computer. It may be argued that the aberrations are not strongly dependent on entrance pupil location for small field angles. The solution is to then move the stop some small distance from the front focal plane, and proceed to evaluate the lens. Though this technique may work during evaluation without introducing nonnegligible errors, it is unsatisfactory during the optimization process. Even with the focal length constrained, the focal distances may change sufficiently to place the focal plane too near the fixed stop. Then the defect function diverges due to lack of length in the computer

word. Prevention of this catastrophe by using judiciously selected instructions for ACCOS II and for ACCOS V is described in the Appendices.

The design approach is to minimize a number of designer selected transverse ray errors. It has been shown (Born and Wolf, 1959, p. 468) that the Strehl ratio (and hence the volume under the optical transfer function) is maximum when the wavefront variance (with respect to a sphere centered at the image) is minimum. The minimization of the mean squared spot size on the image plane for a uniform grid of rays traced through the entrance pupil leads to a geometrically based criterion for the optimization. Between these extremes is the construction of a defect function based on ray aberrations which emulates the minimization of wavefront variance. Implementation of such a defect function is shown in the Appendixes.

The design approach is to minimize the values of transverse ray errors. Implementation of the specifications imposed by the paraxial behavior of the systems is demonstrated for two different lens design programs, ACCOS II and ACCOS V.

Ray fan diagrams and psf cross sections are displayed for evaluation of the various lenses. Figure 1.1 shows the reference aperture intercepts of rays lying in the tangential (meridional) plane. The object point is shown with x = o, z = 0, and y negative. Negative object height is conventional. The coordinate system is right-handed.

Tangential fans are traced from three object points: axial, .7 full-field, and full field. Representative plots are at the left-hand side of Figure 1.2. The axial fan diagram is shown only for positive

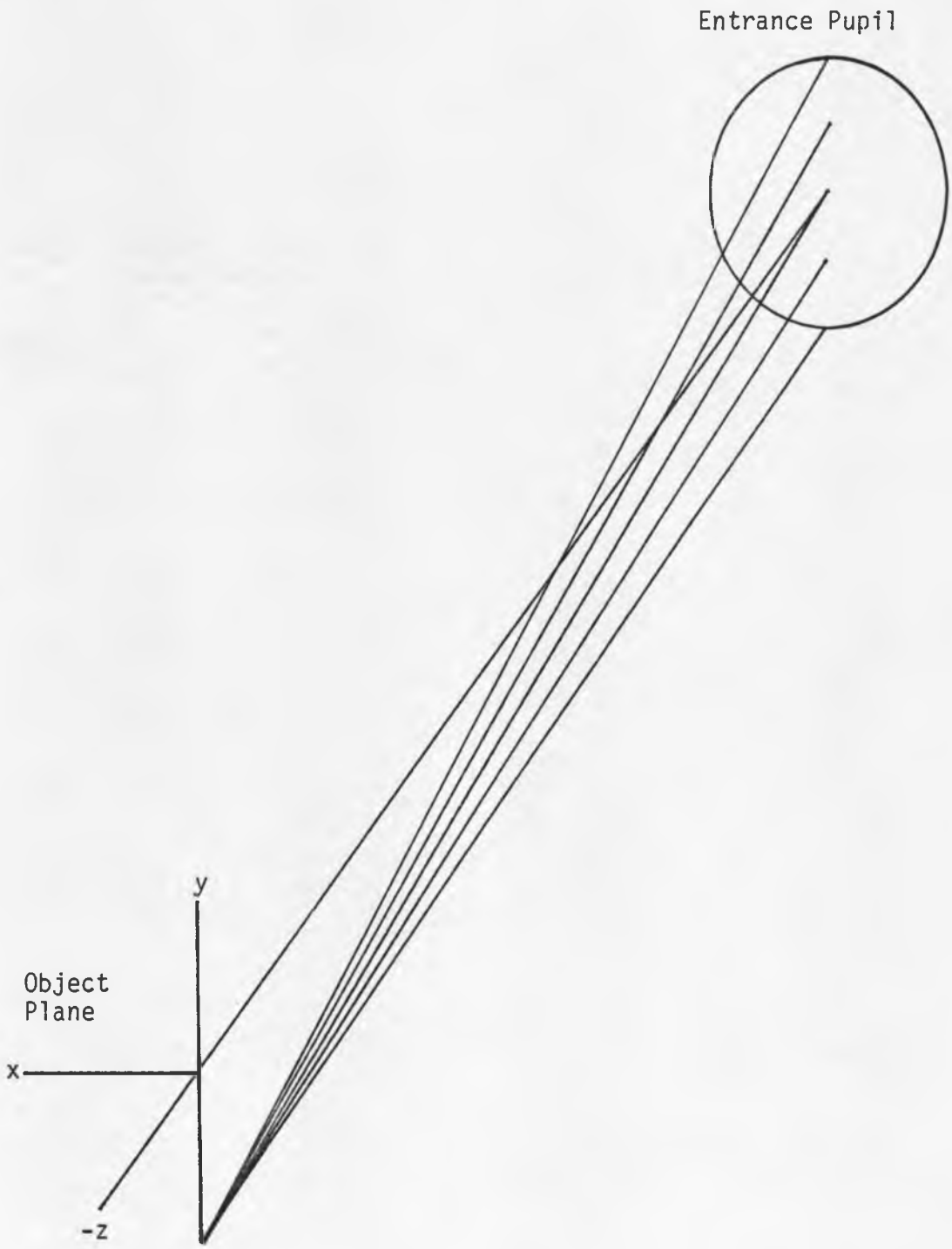

Figure 1.1. A Tangential Ray Fan.

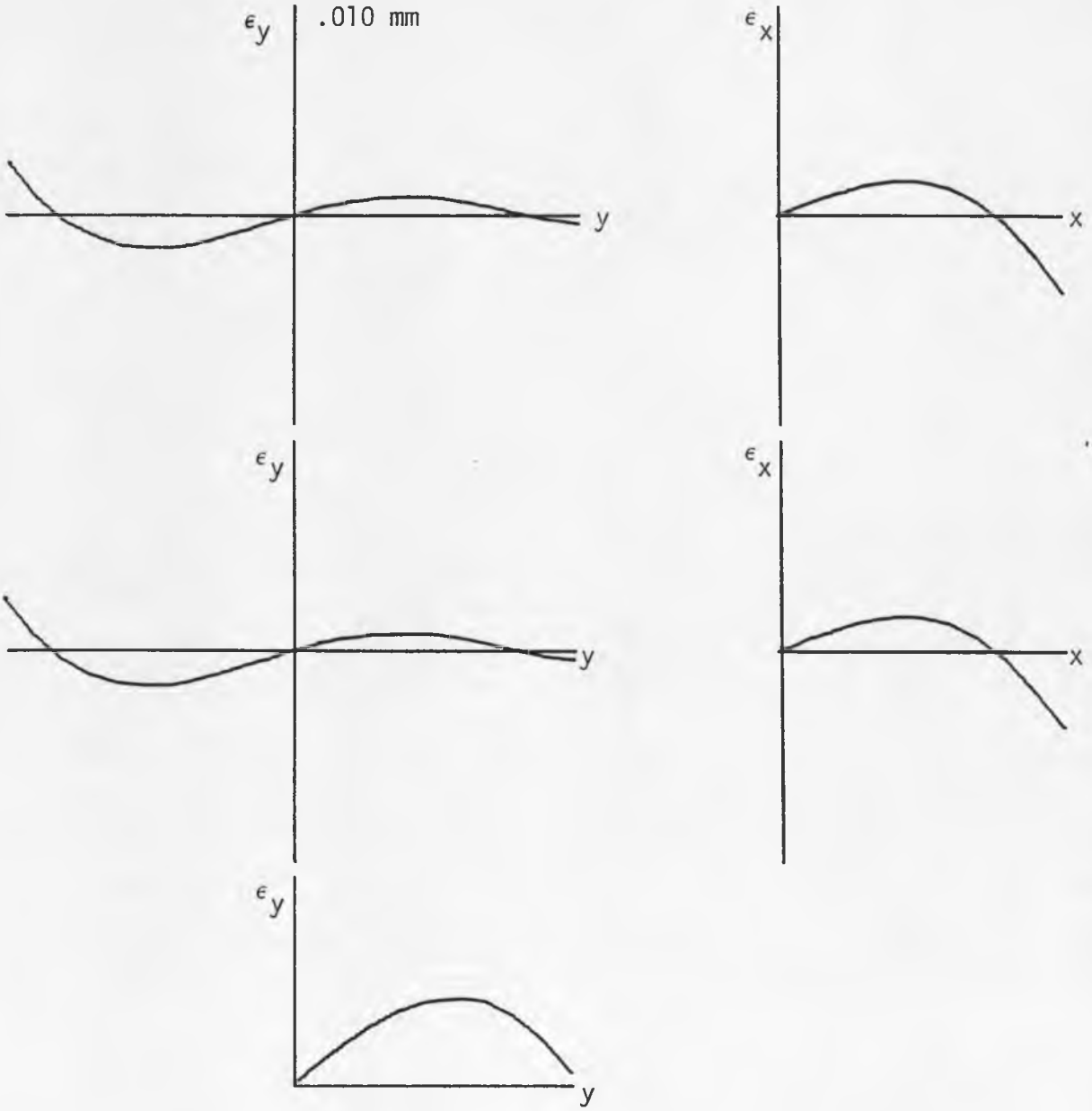

Tangential Fans

Sagittal Fans

Figure 1.2. Representative Ray Fan Diagrams

y coordinate in the reference aperture, because (transverse) axial aberrations have odd symmetry in a bilaterally symmetric system. The origin in a tangential ray fan diagram represents the y-height of the central ray of the fan (chief ray). The horizontal axis in the diagram represents the normalized y coordinate at the reference aperture. The vertical axis in the y fan diagram represents the y-height of a ray at the image plane with respect to the y-height of the chief ray at the image plane. The difference is called ϵ_y.

Figure 1.3 shows some rays forming a sagittal (radial) fan. The rays intersect the entrance aperture along the x-axis. Rays of the tangential fan remain in the yz plane from object to image if the system has reflection symmetry about the plane. However, rays of the sagittal fan fall along a line only to the proximity of the first refracting or reflecting surface. The general case is that the intersections with the first surface do not lie in a plane, due to the curvature of the surface.

For a system with bilateral symmetry, the sagittal fans are shown only for rays traced through the half of the pupil with y = 0 and x positive. The horizontal coordinate is the fractional pupil radius and the vertical coordinate is the x intercept of the ray with the image surface. The pupil coordinate increases to the right in the fan plot. There is usually a difference between the y-height of a sagittal ray and the chief ray height at the image, but this is typically an order of magnitude smaller than the x error, called ϵ_x.

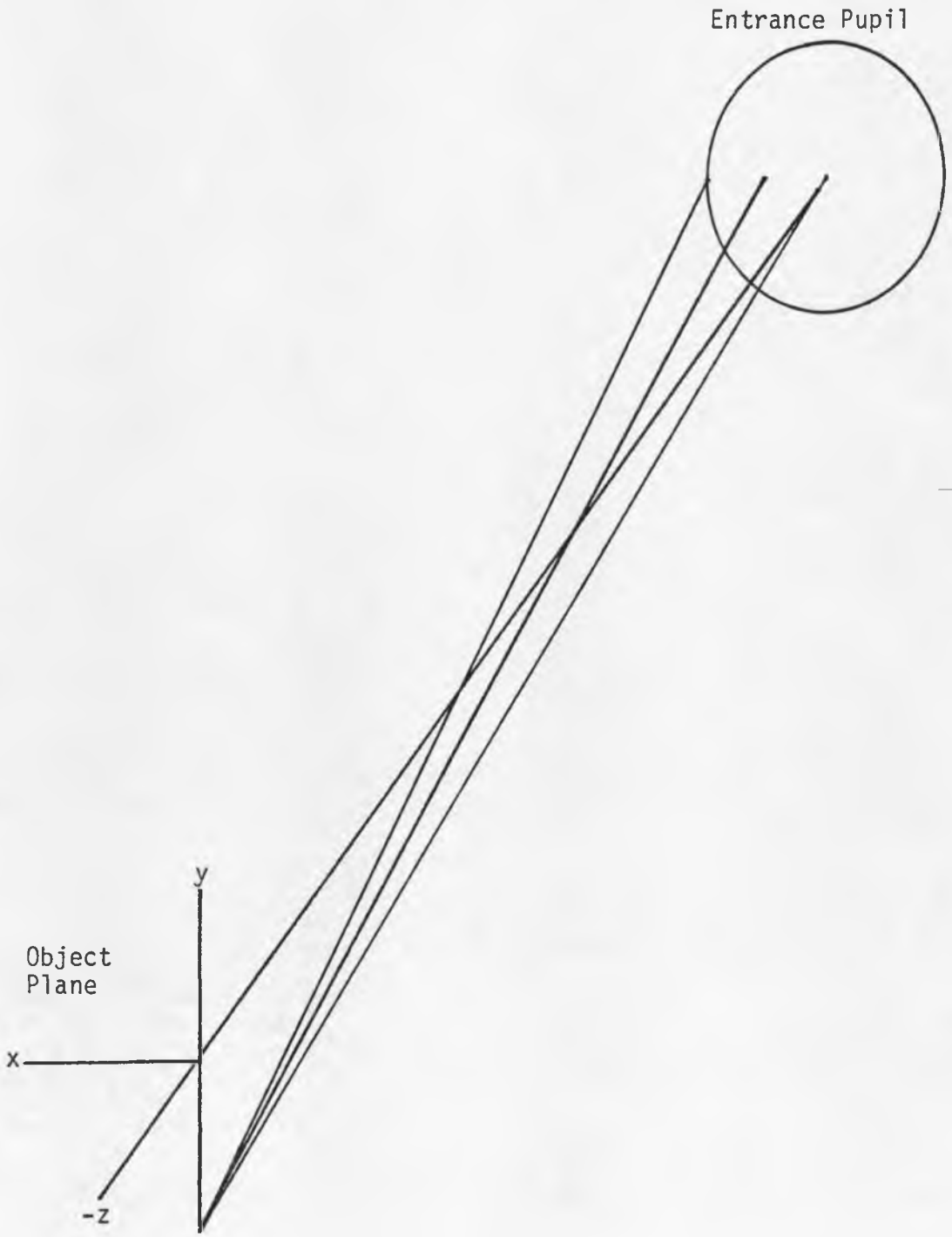

Figure 1.3. A Sagittal Ray Fan.

The sagittal ray fan diagram for an axial object point is identical to the tangential one if the system has rotational symmetry, so only two sagittal ray fan diagrams are shown, one for .7 full field and one for full field. These are at the right of Figure 1.2.

Point spread function calculations are based on the Fresnel-Kirchhoff diffraction formula. From a given object point, ACCOS V uses a two dimensional array of rays to sample the entrance aperture. Optical path differences along these rays are calculated. The differences are then approximated with a polynomial in x and y, and the polynomial is used as the transmittance (pure phase) function in the diffraction integral. Cross sections of the psf for $x = 0$ and for $x > 0$ y = constant at the image plane are calculated. The cross section in the yz plane is shown at the left of the set of diagrams (see Figure 2.4). The right side of the figure gives the sagittal sections. As in the case of ray fan diagrams, symmetry properties of the optical system eliminated the need to plot the sections in their entirety.

An interesting development was the design of an asymmetrical FTL. Such a design was described in a Japanese publication (Matsui, Minami, and Yamaguchi, 1974), but without the values of the construction variables. Here, a lens is described and an evaluation presented. The diffracting aperture for this lens can be kept in the paraxial front focal plane, but the implementation of the optimization is different from the case of the symmetric lens.

Also, the FTL for use with different laser wavelengths is described. If we do not require color correction of the lens in the

conventional sense, but only that the lens be well corrected at several wavelengths independently, with back focal distance and focal length varying with wavelength, then a useful lens can be realized. The means to perform this optimization using the Multiple Configurations Option of ACCOS V is given. Ray trace data and psf calculations show how well the lens suits the requirements at the optimization wavelengths. The feasibility of designing such a lens with only one glass type is demonstrated. The possibility of such a solution has been discussed in several places, and concluded to be doubtful for various reasons.

CHAPTER 2

FOURIER TRANSFORM LENSES

Lenses and Spatial Frequency Mapping

The first order geometrical optics properties of a Fourier transform lens are shown in Figure 2.1. A collimated coherent light beam, parallel to the optical axis, is diffracted at the transparency S. The beam is assumed to be collimated, for a diffraction grating introduces aberrations into diverging or converging light. Also, the diffracting transparency is taken to be in the front focal plane of the lens. For justification of this choice, the reader is referred to Appendix A, where we consider the Fresnel-Kirchhoff diffraction integrals for the Vander Lugt matched filter correlator. The upper and lower rim rays and the central ray (called the chief ray) are shown. The angle they make with the axis at the right of the diffracting plane is the maximum angle of diffraction. If the maximum spatial frequency in S is ξ_{max} and the illuminating wavelength is λ, then the relationship can be written $\xi_{max} = \sin\theta_{max}/\lambda$. This result follows directly from the diffraction grating equation. The rays focus at a height d_{max} above the axis. Only the +1 order is shown, though the maximum spatial frequency also determines a -1 order, which is focused an equal distance below the axis.

Consider a lower spatial frequency $\xi = \xi_{max}/2$. The chief ray for this frequency leaves S at an angle θ, $\theta = \sin^{-1}(\xi\lambda)$. Mutatis

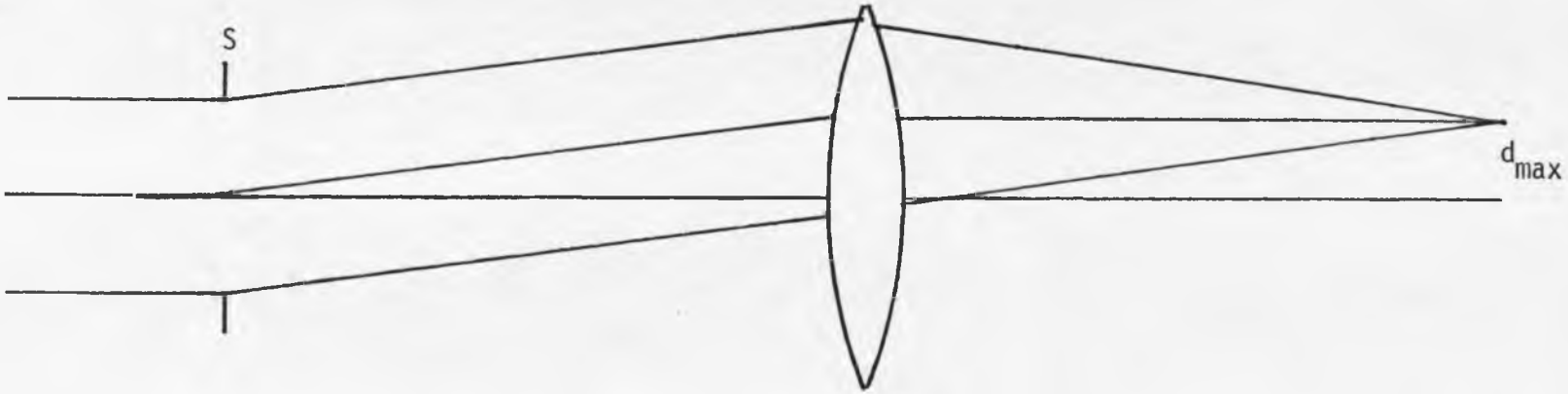

Figure 2.1. Lens with Diffracting Object in Front Focal Plane.

mutandis, we have $\sin\theta = \sin\theta_{max}/2$. To yield the proper metric for Fourier space, $d = d_{max}/2$. The implication of this is that the lens is to linearly relate the transverse displacement in the focal plane to spatial frequency: $d \propto \xi$. The chief ray passes through the front focal plane and emerges parallel to the optical axis. In the paraxial thin lens approximation, it has reached a height of $f\theta$ at the lens, so we have $d = f\theta$. However, ξ is proportional to $\sin\theta$, and so at nonzero spatial frequencies, the difference between $f\theta$ and $f\sin\theta$ represents a departure from the ideal FTL. A photographic objective typically has a $d = f\tan\theta$ scaling in the image plane, where θ is the semifield angle. We shall comment later on the $(\sin\theta - \tan\theta)$ difference.

Marginal and Chief Rays for a Fourier Transform Lens

The chief ray traveling at angle θ crosses the axis at the diffracting aperture, so the diffracted light appears to be coming from an infinitely distant object, with the aperture stop at the diffracting aperture. This holds for the continuum of angles from $-\theta$ to $+\theta$, so the description of this feature of a FTL is the same as that for an image forming lens viewing an infinitely distant monochromatic object field, with field of view 2θ, having the aperture stop in the front focal plane. In the FTL, parallel rays in object space represent light diffracted by a particular spatial frequency component in the diffracting plane, and in the image forming lens, parallel rays represent light from the same infinitely distant field position. Thus, the same design procedures are usable for FTL design as are used for the design of imaging lenses, so long as the object-pupil and image-transform dualities are understood.

However, implementation of the procedures may be quite difficult. The defect functions employed in the optimization are different, of course, for the performance requirements are different.

In Figure 2.2, the marginal ray and the chief ray for a lens are depicted. The marginal ray leaves an axial object point infinitely distant, passes through the edge of the aperture stop, and intersects the optical axis again at the paraxial focal plane. The chief ray leaves a point at the edge of the field of view and passes through the center of the stop. The stop is located at the front focal plane of the lens, so the ray is parallel to the axis to the right of the lens. With the chief ray normal to the focal plane (viz., the lens is telecentric in image space), there is no explicit dependence of the psf on spatial frequency (field angle). Therefore, if the aberrations do not change with field angle in object space, the system is isoplanatic, whether or not it is aberration free.

If the chief ray is not normal to the focal plane, the wavefront is converging at a nonzero angle from the normal, and so even a perfect wavefront will form an irradiance pattern with an elliptical shape for the Airy disk. For an off axis object point in the yz plane, the x dimension of the psf will be constant, but the y dimension will change with the cosine of the field angle, even when the wavefront is spherical. Thus, the system is not isoplanatic, though this may admittedly be inconsequential.

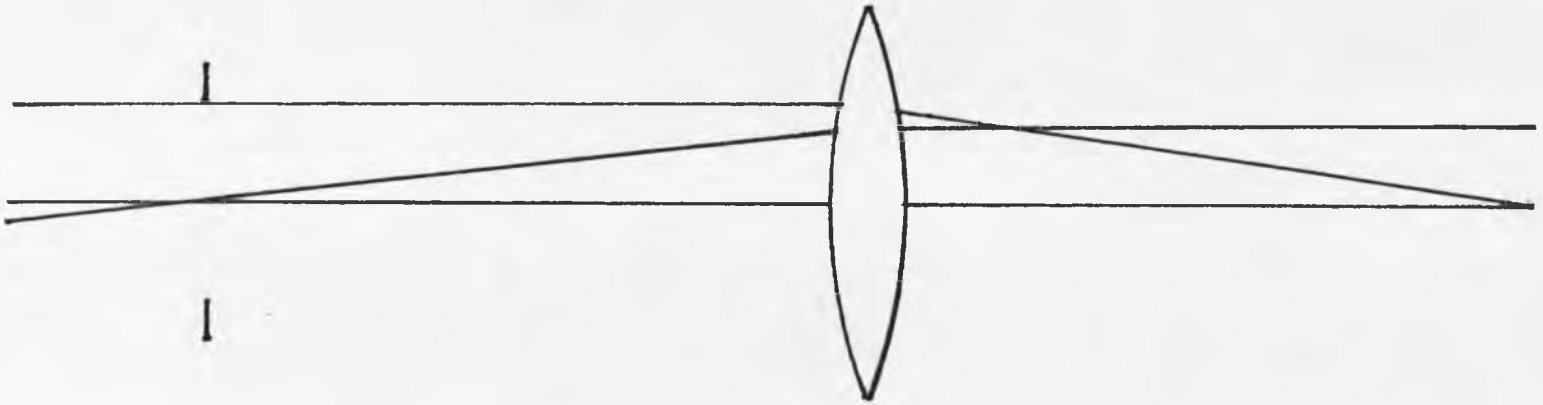

Figure 2.2. Marginal Ray and Chief Ray of a Lens with Aperture Stop in Front Focal Plane.

Cemented Aplanat as a Fourier Transform Lens

Before discussing the design of a Fourier transform lens, let us see how well a doublet telescope objective satisfies the requirements delineated up to this point. A focal length of 235 mm, helium-neon laser illumination (632.8 nm), and an input format of 18 mm radius containing Fourier components up to 30 lp/mm were selected as parameters for the design and evaluation of the lens for the single wavelength problem treated in this chapter. To gather all the light diffracted by the transparency at S (see Figure 2.1), the lens must have a clear aperture radius larger than the radius of S by an amount $f\tan\theta_{max}$, where f is the distance to the lens and θ_{max} is the maximum angle of diffraction.

For a maximum spatial frequency of 30 lp/mm and a wavelength of 632.8 nm, we find that $\theta_{max} = \sin^{-1}(\frac{30}{mm} \times 632.8 \times 10^{-9}) = 1.1°$. Assuming that the front focal distance is about 235 mm, we have $f\tan\theta_{max} = 4.5$ mm. Thus, the lens must have a 22.5 mm clear aperture radius. The transparency has a diameter of 36 mm and the lens has a diameter of 45 mm. The nine millimeter difference in diameter allows all the light diffracted by Fourier components up to 30 lp/mm to be collected by the lens.

Design of a Cemented Aplant

A cemented doublet with the stop at the lens can be corrected for spherical aberration and axial color (chromatic variation of back focal distance). If the designer is free to choose glass types, the coma can be suppressed and possibly eliminated. The stop is placed at the

lens for use as a telescope objective. The doublet is to be used later as a FTL with clear aperture diameter of 45 mm and efl of 235 mm. With the stop located at the lens, the stop must have a diameter of 45 mm to allow use of the entire lens clear aperture. This yields a focal ratio of F5.2. Typical angular field diameter listed by one manufacturer for a doublet of this focal length and focal ratio was 3.5°, so the achromat was designed to cover this field angle. (When the lens is evaluated as a FTL, the stop is moved to the front focal plane and the stop diameter is reduced to 36 mm. The lens diameter is constant; the focal ratio increases from F/5.2(235/45) to F6.5(235/36).) Selection of glasses from the Schott list of preferred glasses was made after the design was initially optimized by the lens optimization program ACCOS V. These considerations were made so that this design would represent a cemented achromat of high quality, readily available to the coherent optics experimenter.

The optimization of this lens was based on an exact ray trace. Spherical aberration and axial color were minimized using three zonal rays, and the coma was minimized by comparing the average of full field upper and lower rim rays with the chief ray. The primary wavelength for the design was 587.6 nm, a customary choice for visual optics. Table 2.1 contains a description of the lens.

Evaluation of a Fourier Transform Lens

In order to evaluate the doublet as a Fourier transform lens, the stop was moved to the front focal plane. Selection of the best transform plane, nearer the lens than the paraxial back focus due to

Table 2.1. Cemented Aplanat as a Fourier Transform Lens.

Radius (mm)	Thickness (mm)	Glass Type
	10^{10}	Air
Stop	233.1593	Air
173.6676	9.4	SK5
-83.0344	2.35	SF12
-405.2721	229.19885	Air

EFL at 632.8 nm = 234.9475 mm
Paraxial back focal distance = 229.3353 mm
Paraxial front focal distance = 233.1593 mm
Program was given a field angle of 1.08849° = $\tan^{-1}$ .019
Paraxial chief ray height at paraxial focus = 4.46400 mm
Real chief ray height at best focus = 4.46175 mm
$f\sin\theta$ = 234.947sin1.08849° = 4.46320 mm
Airy disk radius = 0.005 mm

undercorrected field curvature and astigmatism, was done by using a defect function developed for the optimization of a FTL (see Appendix A). The only parameter allowed to vary during this optimization was the distance from the lens to the transform plane. The paraxial back focal distance of the doublet at 587.6 nm is 229.382 mm; at 632.8 nm, it is 229.335 mm, and the selected back focal distance was 229.199 mm.

The ray fans in Figure 2.3 and the cross sections of the point spread functions in Figure 2.4 were calculated for this plane. The ray fans are for axial, .7 full field, and full field objects. Tangential fans are traced from the bottom to the top of the entrance pupil; sagittal fans are traced from the center to a value of +1 in the normalized pupil. (The program recognizes object heights, viz., tangents of angle.) The chief ray heights at this plane for the two field angles are 3.12404 mm and 4.46175 mm. The full field angle of $\tan^{-1}$ .019 corresponds to 30 lp/mm. The field angle is measured as a tangent, so the .7 full field angle is .76199°. The distortion measured by consideration of the chief ray intercept with the best focal surface shows that the differences are inconsequential in this instance. However, an interesting and salient feature of the problem is displayed graphically in Figure 2.4. The vertical line at the center of the cross sections represents two parameters. Its location corresponds to the intersection of the chief ray with the selected focal surface, and its height represents the irradiance in the point spread function of an aberration free system. Note that at the focal points for the off axis angles (nonzero spatial frequencies) that the psf's are not maximized at the chief ray location.

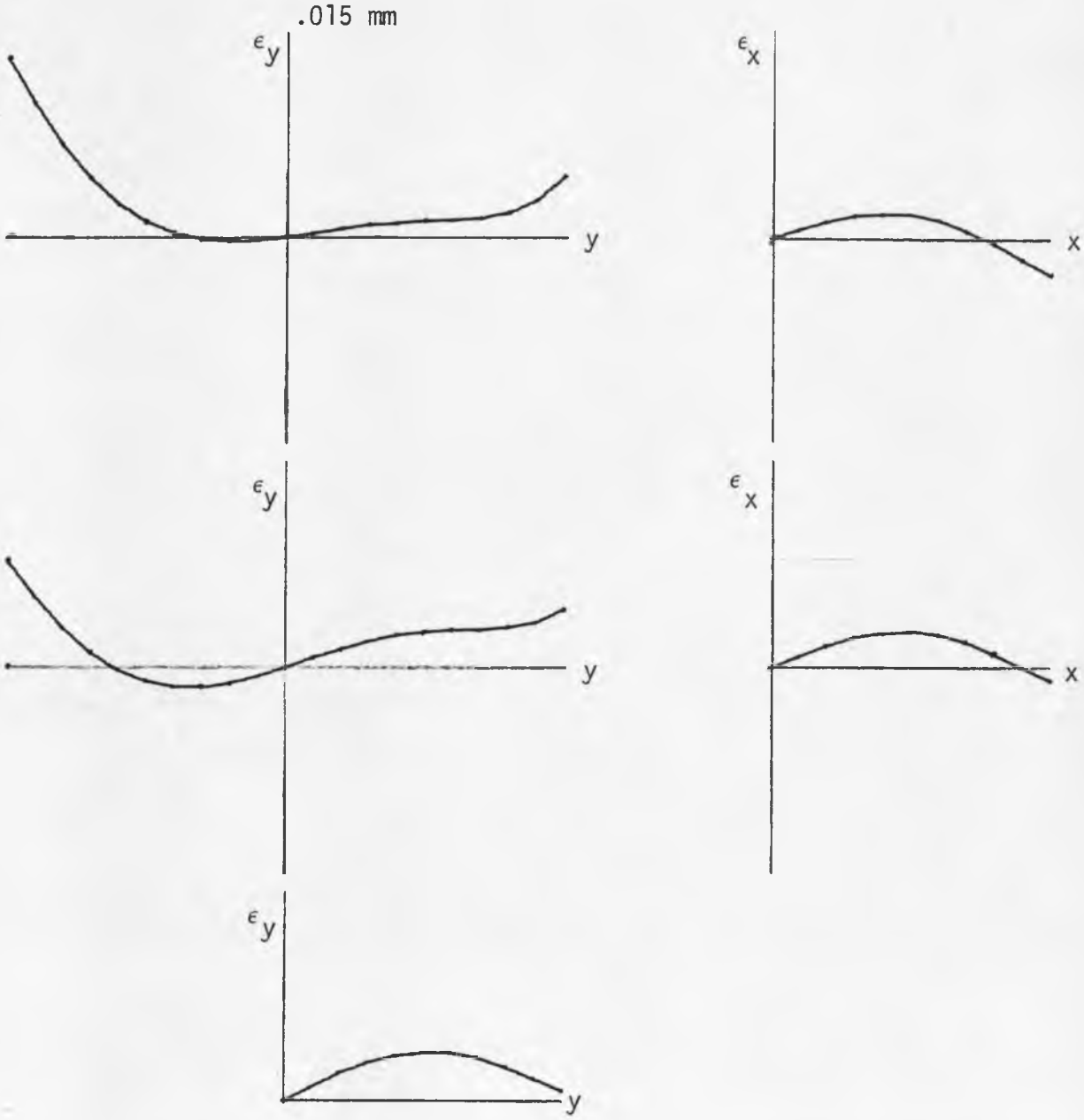

Tangential Fans

Sagittal Fans

Figure 2.3. Ray Fans for the Cemented Aplanat.

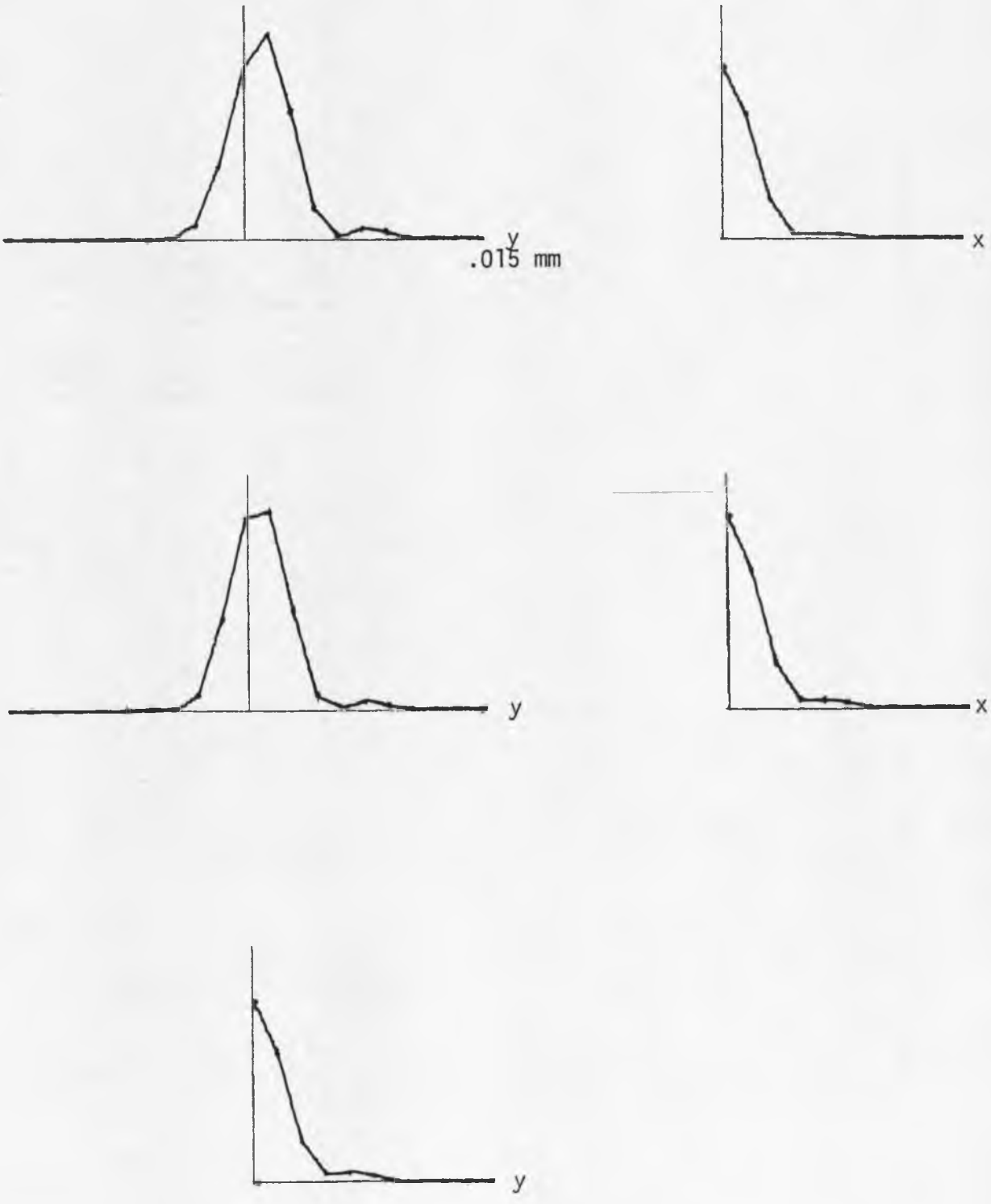

Figure 2.4. PSF's of the Cemented Aplanat as a Fourier Transform Lens, F6.5.

Thus, we see that it is deceiving to measure either distortion or ($\sin\theta$ - $\tan\theta$) in terms of chief ray intercepts. The chief ray is not identified by a detector; the irradiance is the quantity measured.

In his study of holographic matched filter correlators, Fienup (1977) has shown the relevance of wavefront variance in evaluating system performance. The processor is designed to form the autocorrelation of the input to which the filter is matched. He shows that the ratio of the peak value of the irradiance in this autocorrelation to the theoretical maximum is a linear function of wavefront variance. The dependence on the variance is identical to the Strehl ratio relation (Born and Wolf, 1959, p. 468), but the criterion for acceptability is different. Fienup assumes that an irradiance of one-half will allow detection of the autocorrelation. At this level, the equation relating the ratio to the wavefront variance becomes inaccurate to the extent that a digital model is required.

Using a quasi-random object and a computer model of the processor, he shows the autocorrelation of the object for phase errors through sixth order with standard deviations as large as one wavelength. From these simulations, it can be deduced that "a standard deviation of 1/8 wavelengths of phase error results in a greatly reduced, but still detectable autocorrelation peak." Also, "a standard deviation of 1/4 wavelengths results in an autocorrelation peak that would be lost in the noise."

Although the peak phase error corresponding to a standard deviation of $\lambda/8$ depends upon the order of the aberration, the

autocorrelation seems to be fairly independent of the aberration type when the standard deviation is this small.

Fienup's treatment deals only with the ratio as a function of the first Fourier transforming element's effect on wavefront variance. The wavefront variance for the second lens of the correlator is assumed to vanish. From his treatment, we deduce then that the Fourier transform lens must have a standard deviation no worse than $\lambda/8$. If the wavefront is worse than $\lambda/8$ standard deviation, then an imperfect second element assures unsatisfactory performance.

We note that a standard deviation of $\lambda/8$ corresponds to a Strehl ratio of 0.383. The level of acceptability for an imaging lens is often taken to be $\lambda/14$ standard deviation, or a Strehl ratio of 0.8. We see that the cemented aplanat given in the table satisfies even the stronger of these criteria.

The requirements to yield a Fourier transform in the rear focal plane created no need for the lens to be symmetric. Fourier transform lenses are often seen with $f\sin\theta = R$, the input format radius (Blandford, 1970; von Bieren, 1971; Steel, 1974; Wynne, 1974 a, b). However if the maximum spatial frequency of interest is ξ_{max}, we note that the Fourier transform format is of radius $f\lambda\xi_{max}$, regardless of R.

CHAPTER 3

THE VANDER LUGT MATCHED FILTER CORRELATOR

Geometrical Optics of the Correlator

Figure 3.1 represents the geometrical optics of the Vander Lugt filter correlator. Input to the correlator is located in the plane S_1. It is the front focal plane of lens L_1. The Fourier transform plane is at S_2. The clear aperture of S_2 represents the transmission hologram (matched filter) which is to be illuminated with the Fourier spectrum of the input. It lies in the front focal plane of L_2. The lens L_2 will Fourier transform the amplitude transmitted through S_2 and form a convolution, a cross correlation, and an image at S_3 (Goodman, 1968, p. 176).

In presenting this ray treatment, we could assume that the reference beam angle used in exposing the matched filter was zero. In actuality a prism and a tilted plate assembly are introduced between the hologram and L_2 in order to bring the axis of the beam leaving the filter into coincidence with the optical axis. We thus reduce the clear aperture and the field angle requirements on the second lens. This is especially important in the case where the filter is rotated in order to implement an orientation search for a matching signal. To see this, consider an input which is matched to the filter. Also, consider the input to be on axis; then the collimated beam emanating from S_2 is focused at S_3 and forms the autocorrelation of the input convolved with

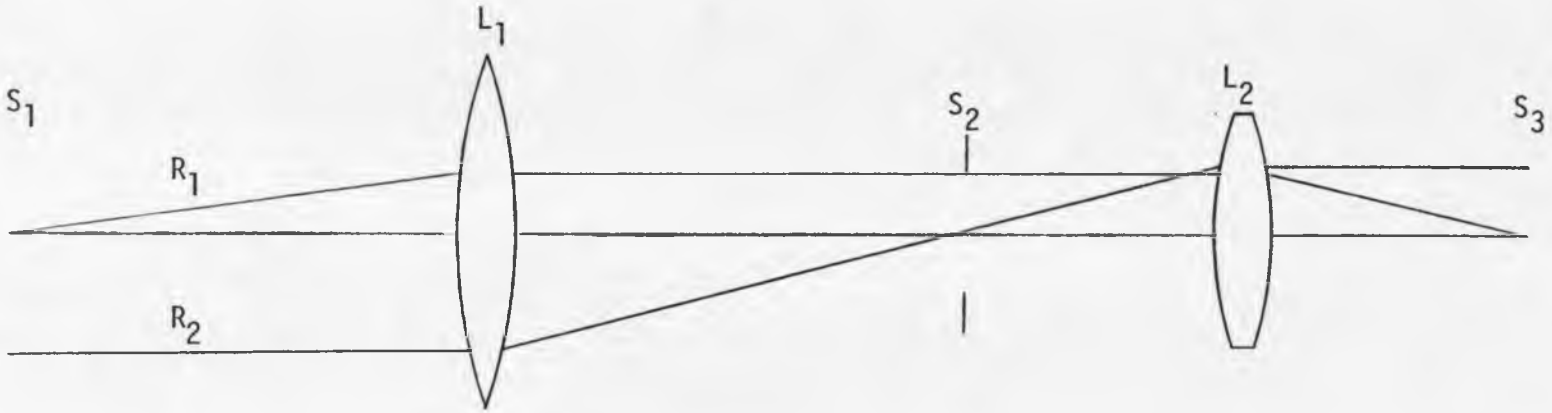

Figure 3.1. Marginal Ray and Chief Ray for Coherent Imaging in the Correlator.

the psf of the optical system. This autocorrelation appears off the axis in S_3. Now if a prism is introduced to refract the beam coming from S_3 into parallelism with the axis, and a tilted plate brings it into collinearity with the axis, the autocorrelation appears on axis. The autocorrelation lies in the same plane as the image. Therefore, we examine the performance of the system by looking at the imaging psf of the optics. (We assume the prism and plate, as optically perfect and powerless elements in a collimated beam, introduce no aberrations.) The psf's at S_3 for off axis points in S_1 tell us whether the Vander Lugt optics truly form a shift invariant system (Goodman, 1968, p. 194, Problem 7). For a discussion of the locations of the correlator's focused light, we refer the reader to Appendix A.

Ray R_1 emanates from the axis. It reaches L_1 at a height such that it meets the hologram at its edge. The ray continues to S_3. S_1 is in the front focal plane of L_1, so the ray is parallel to the axis after refraction and therefore crosses the axis again at the rear focal plane of L_2. Its intersection with the axis locates the image of S_1. A second ray begins at the edge of the input format and is parallel to the optical axis. Because S_2 is the front focal plane of L_2, the ray leaves L_2 parallel to the axis and reaches S_3 at a height determining the edge of the output format. The lenses are arranged with their foci coincident at S_2, giving an afocal imaging system. The transverse magnification of such a system is proportional to the ratio of focal lengths.

Magnification = - focal length of L_2/focal length of L_1.

Now we can discuss the design field angle and f-ratio requirements for L_2 to work with L_1. The f-ratio of L_1, N_1, was determined from the chosen focal length, f_1, and the desired input format diameter, D_1. $N_1 = f_1/D_1$. R_2 is parallel to the optical axis to the left of L_1, and passes through the edge of the input format. Therefore, it is a marginal ray for L_1, and the angle it makes between L_1 and L_2 is the numerical aperture of L_1. L_2 is to Fourier transform the amplitude transmittance of S_2, for S_2 lies in its front focal plane. As seen in Chapter 2, S_2 is now considered the aperture stop for L_2, and R_2 is a chief ray for L_2. As a chief ray, its angle with the axis at S_2 (which is also L_2's entrance pupil) is the field angle for L_2. Thus, the angular field of view for L_2 was not a free variable once the f-ratio of L_1 was determined.

R_1 passes through the edge of S_2 and is a marginal ray for L_2. The size of the aperture stop at S_2 for L_2 was determined by ξ and f_1. The numerical aperture of L_2 now depends solely on the choice of the focal length of L_2, f_2. However, f_2 may have been chosen by the detector size, for the detector can be no smaller than $D_1 \cdot f_2/f_1$, as seen from the equation for afocal transverse magnification.

Figure 3.2 shows a cone of rays constructed about the ray R_2 of Figure 3.1 to represent imaging from the edge of the input. In performing as a FTL, L_1 had to form an image from rays leaving an object infinitely distant to the left. As a part of the correlator, it must collimate rays leaving a point of S_1. L_2 forms an image of a point which is (apparently) infinitely distant. It need not be symmetrical.

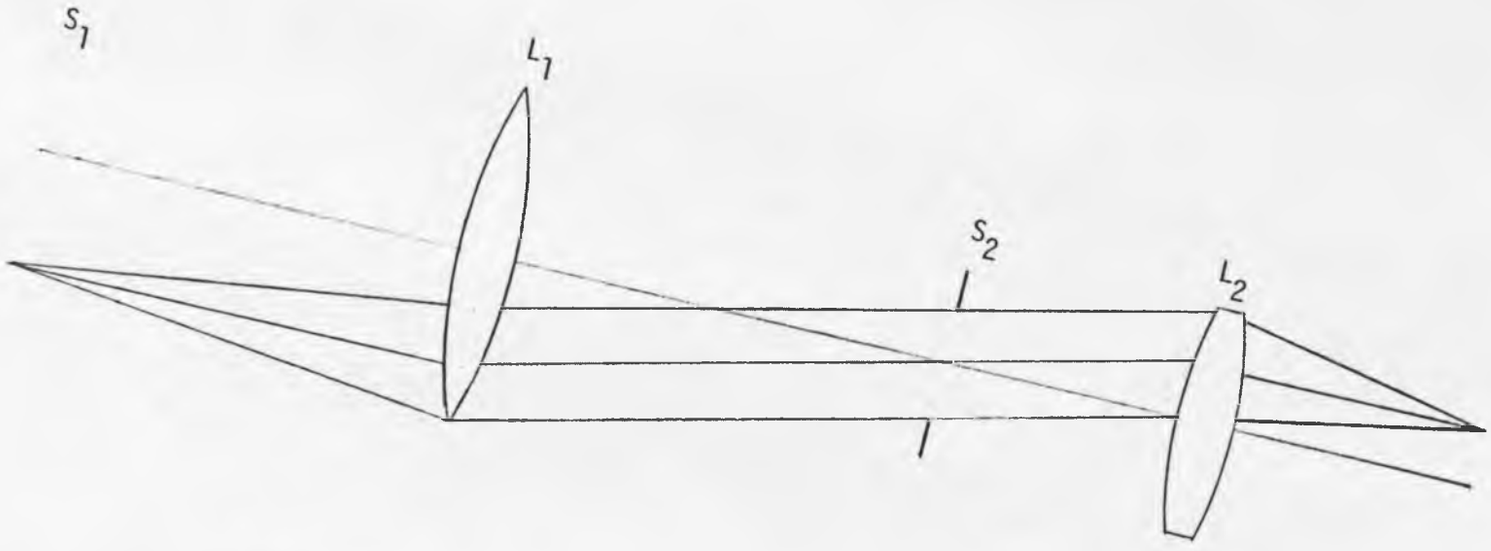

Figure 3.2. Imaging from Input Transparency to Detector Plane.

Doublets as the Correlator Lenses

Table 3.1 describes a pair of doublets arranged in the afocal imaging configuration. The common focal point is what would ordinarily be the rear focal point of each of the lenses. The rays traced for analysis are traced from three points in the input plane. The first point is on axis, the second is 12.6 mm below (.7 field), and full field rays are traced from 18 mm below the axis. This choice of inverted object is merely a lens designers' convention. Two fans of rays are traced from each point. The y-fan fills the meridional diameter of the hologram aperture at S_2, and the x-fan covers the left half of the sagittal diameter.

The plane of S_1 is the paraxial (at 632.8 nm) front focal plane of L_1. S_2 lies as the distance selected by defect function given in Appendix A, with L_1 described as a FTL. The lenses are arranged symmetrically about S_2. (Reversing the orientation of the second doublet is not of much interest.) S_3 was selected by a similar ACCOS V defect function, but with the field of view and object location being determined by the input format rather than by ξ. Also, the aperture stop for this optimization lies at S_2. Because of undercorrected field curvature, S_3 lies closer to L_2 than S_1 lies from L_1.

The system is doubly telecentric and can lead to previously mentioned difficulties in evaluation. Given in Appendix B is a set of ACCOS V card images which will not induce any difficulties. Some versions of ACCOS II required the user to aim rays at the first glass surface, examine their intersections with S_2, and reaim them. Also,

Table 3.1. Cemented Aplanats in Imaging Configuration.

Radius (mm)	Thickness (mm)	Glass Type
	233.1593	Air
173.6676	9.4	SK5
-83.0344	2.35	SF12
-405.2721	229.199	Air
Stop	229.199	Air
405.2721	2.35	SF12
83.0344	9.4	SK5
-173.6676	231.4724	Air

Airy disk radius = .020 mm

construction of an ACCOS II defect function to select best focus of the doubly telecentric system was not a task which could be fully controlled as with ACCOS V.

ACCOS II used a left handed coordinate system. The y-axis was vertical and the z-axis was the optical axis. The x-axis was positive to the right, as we looked along the positive z-axis. It became customary to plot the sagittal ray fans for just the right half of the pupil for circularly symmetric optical systems. ACCOS V uses a right-handed coordinate system, with x increasing to the left. The sagittal ray fans are still plotted with x = 0 at the left edge and x = 1 at the right edge of the normalized pupil (horizontal) axis.

Comparing the ray fans in Figure 3.3, one can see that there is a significant amount of field curvature and astigmatism in the system. The psf's in Figure 3.4 show, as we expect for a symmetric system, no coma, but large amounts of even aberration terms. (The Airy disk radius is .020 mm.)

We have now seen a lens which behaved reasonably well as a FTL failed to satisfy requirements in the correlator configuration. When required to form good images for two pairs of conjugates, the lens failed, for it had not been designed for such an application. Now consider the design of a lens able to focus light from one direction (Fourier transform the input) and also able to collimate light coming from points in its front focal plane (first half of correlator's imaging pair). Also, if the lens is to be used to make matched filters, it must have a back focal distance large enough to allow a reference beam to

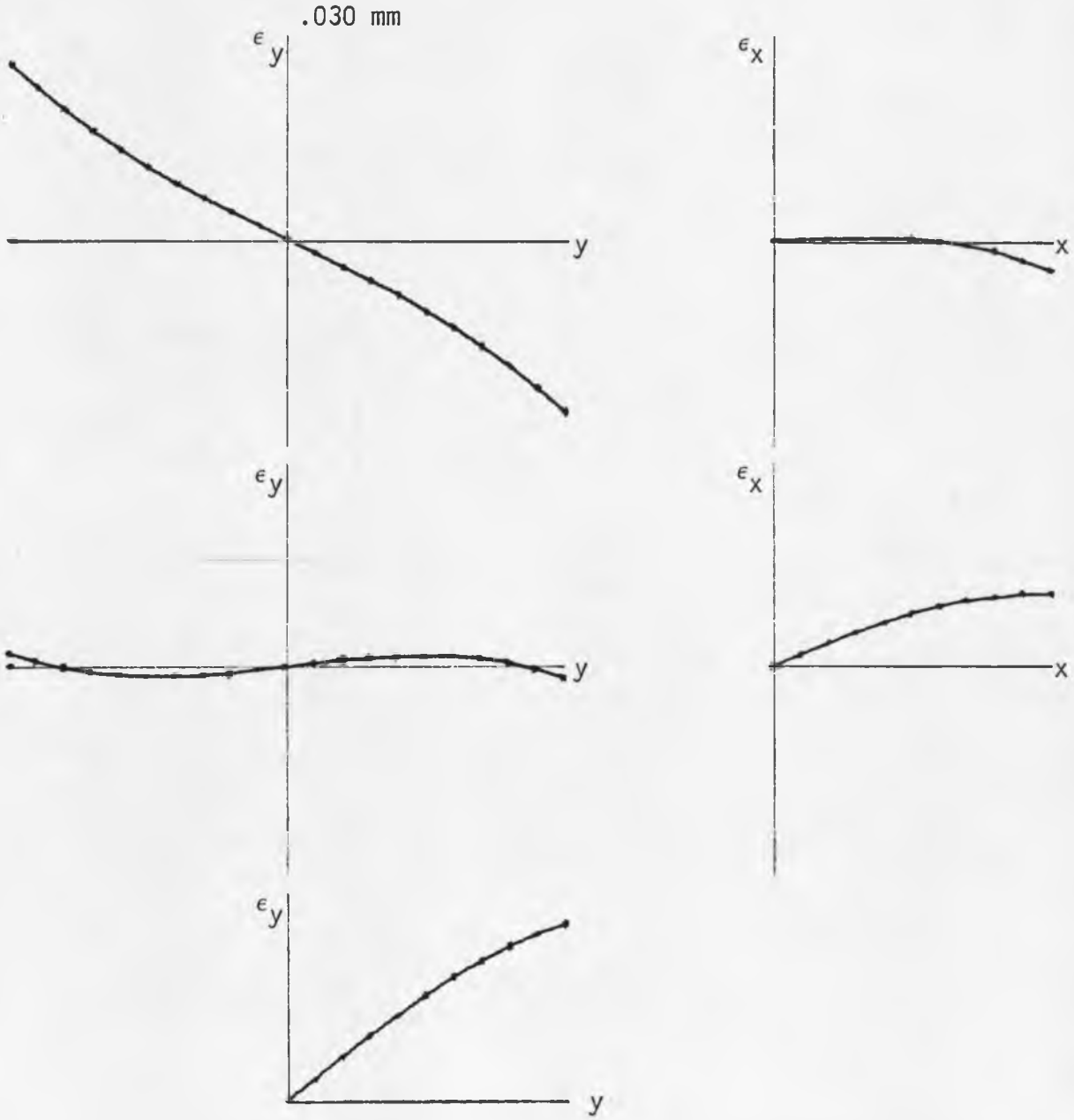

Figure 3.3. Ray Fans for Aplanats in Imaging Configuration.

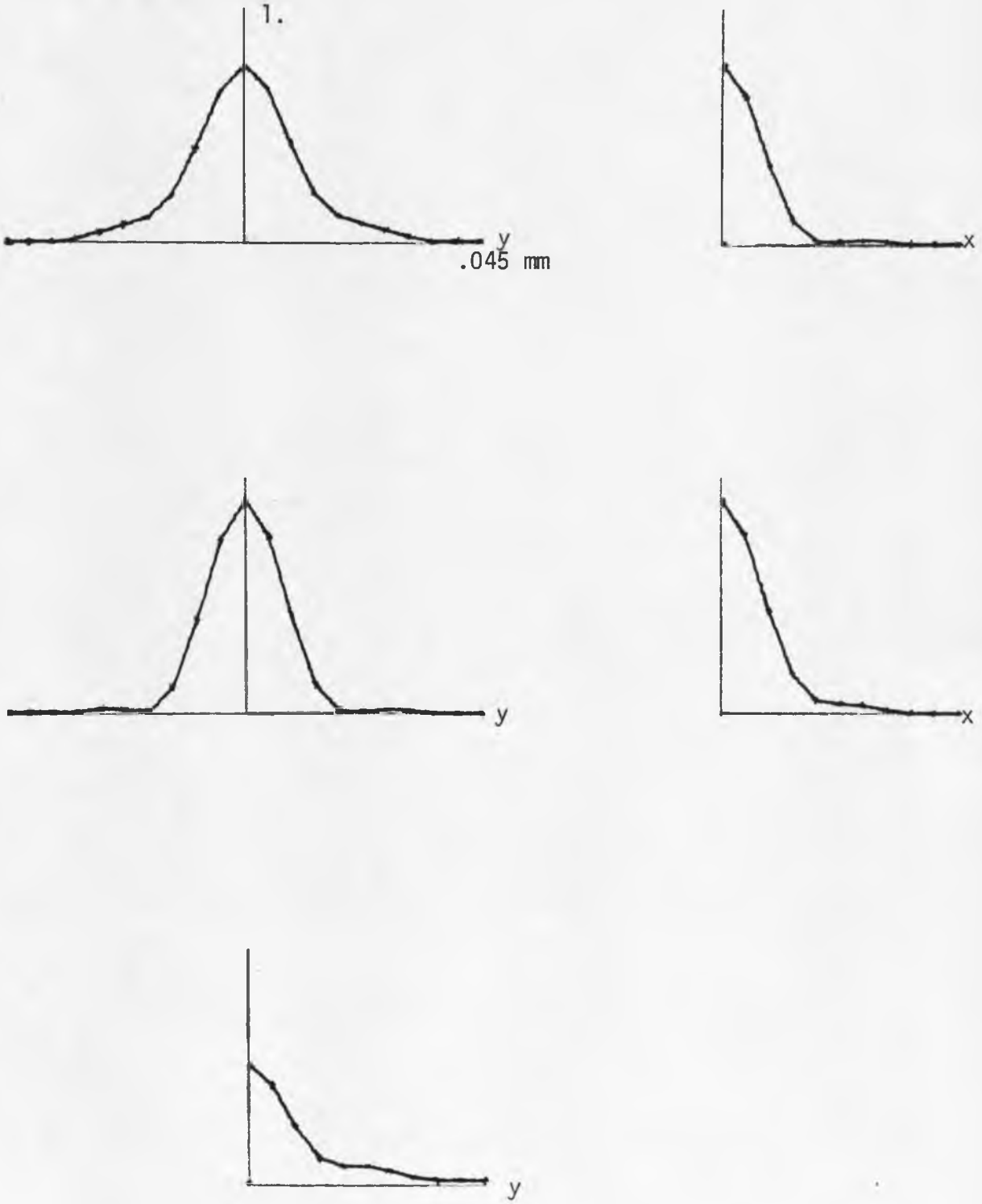

Figure 3.4. PSF's of the Aplanats in Imaging Configuration, F26.

illuminate the Fourier spectrum of the input. (The selection of back focal distance is a function of input diameter size, spatial frequency, and reference beam angle. The relationships are easily understood and best investigated with a diagram. We will assume here that the reader can determine the limits on the back focal distance and then implement them as constraints on the optimization.)

Unequal Focal Length Lenses

Though the input diameter of 36 mm is different from the spectrum diameter of 9 mm, the next lenses were optimized as symmetrical lenses. This insured that the performance in both directions would be good. A lens input description is given in Appendix B. The input location (stop) and Fourier plane were automatically kept symmetrically located about the lens. The defect function was evaluated at a plane different from the paraxial plane, its location determined by the optimization process.

A second lens of shorter focal length, with field angle determined from the f-ratio of the first, was also designed. It has already been shown that the spectral mapping requirements could be satisfied much more easily than the telecentric imaging, so the evaluation presented here includes only the latter for these two lenses. Note that the second lens is not merely a scaled down version of the first lens. Its field angle and numerical aperture are different from the first, so the optimization produces a distinctly different lens.

The relationships of field angles and f-ratios were mentioned earlier. We will use this pair as an example. For L_1, the input

diameter = 36 mm and focal length = 235 mm. This gives an f-ratio of 6.5. (The numerical aperture is .076.) The limit on output diameter was 13 mm. So we find the focal length of L_2 to have an upper limit of 85 mm (13/36 x 235). We know that the input spatial frequency extends to 30 lp/mm, so the spectrum has diameter 9 mm ($2 \cdot 30 \cdot 6.328 \cdot 10^{-4}$ mm). This means L_2 will have an f-ratio of 9.4 or faster (85/9). The field angle for L_2 is .076 or about 4.4°. (Note also that $\tan^{-1}(1/2 \times 13/85) = 4.4°$.) Back focal distance constraints were determined by reference beam requirements and electromechanical devices for the correlator. The lens system description is given in Table 3.2. The evaluations are seen in Figures 3.5 and 3.6. A comment on the diffraction integrals for this configuration is given in Appendix A.

It was mentioned at the end of the first section of this chapter that one could design the second lens without regard to symmetry. All that is required is that the second lens be corrected with the aperture stop at the hologram position in the front focal plane. Such a configuration is still telecentric and afocal, with the same Fresnel-Kirchhoff integrals as the fully symmetric configuration.

Asymmetric Lenses

The design of an asymmetric lens which images well for two sets of conjugates can be done automatically by some optimization programs. There is the restriction, however, that the foci be accessible. Even then, it may prove impossible to impose the constraints necessary to make the lens fit the application. Because the Vander Lugt correlator

Table 3.2. Unequal Focal Length Lenses in Imaging Configuration.

Radius (mm)	Thickness (mm)	Index at 632.8 nm
	191.372	Air
124.3725	10.	1.77866
-923.249	24.8036	Air
-141.441	10.	1.77866
141.441	24.8036	Air
923.249	10.	1.77866
-124.3725	191.372	Air
Stop	69.3718	Air
65.2574	5.	1.77866
-126.774	6.4078	Air
-62.3629	5.	1.77866
62.3629	6.4078	Air
126.774	5.	1.77866
-65.2574	69.3401	Air

EFL of first triplet at 632.8 nm = 234.3956 mm
Paraxial back focal distance = 191.4421 mm
EFL of second triplet at 632.8 nm = 82.145367 mm
Paraxial back focal distance = 69.494597 mm
Airy disk radius = .007 mm

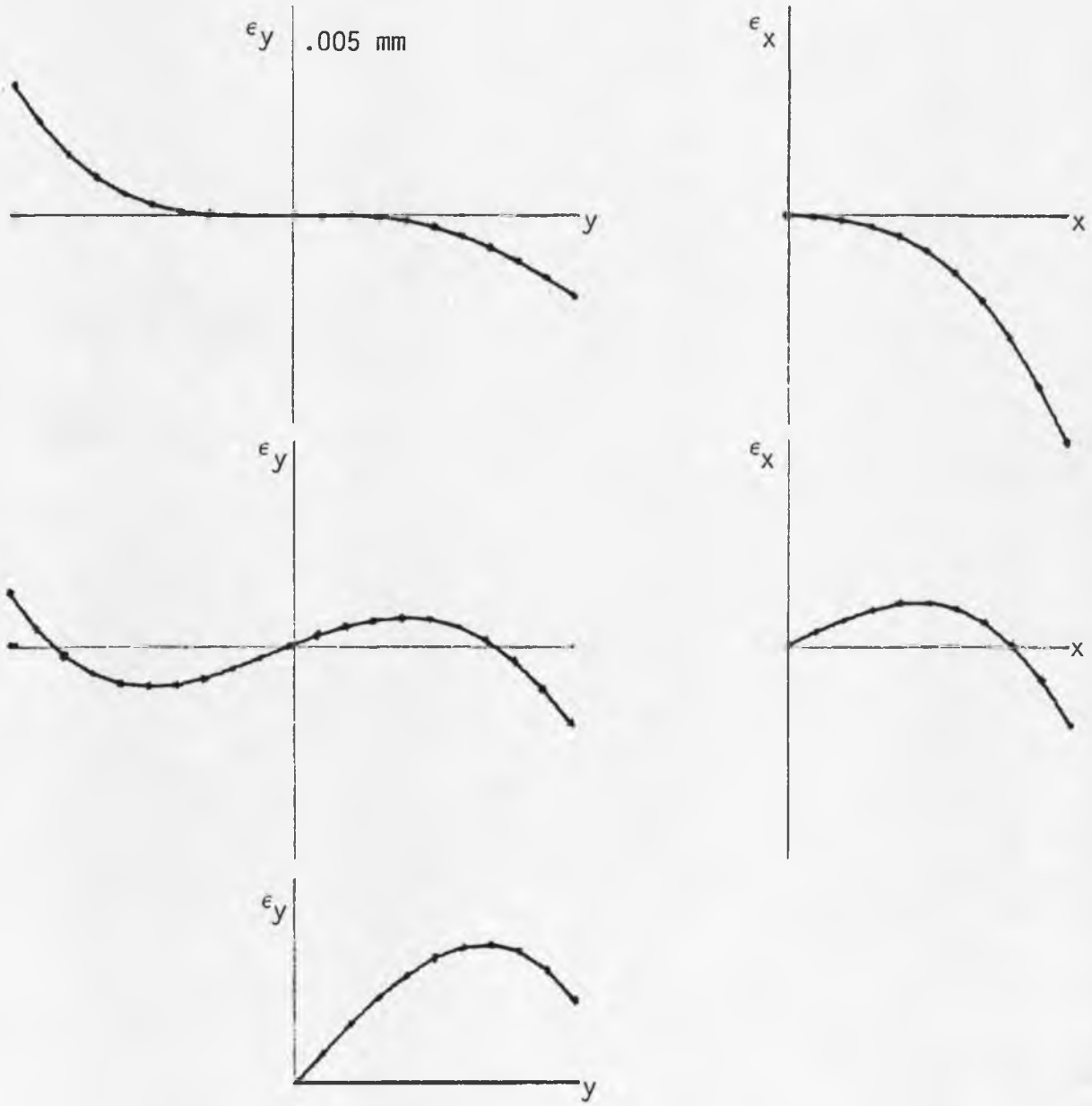

Tangential Fans

Sagittal Fans

Figure 3.5. Ray Fans for Unequal Focal Length Lenses.

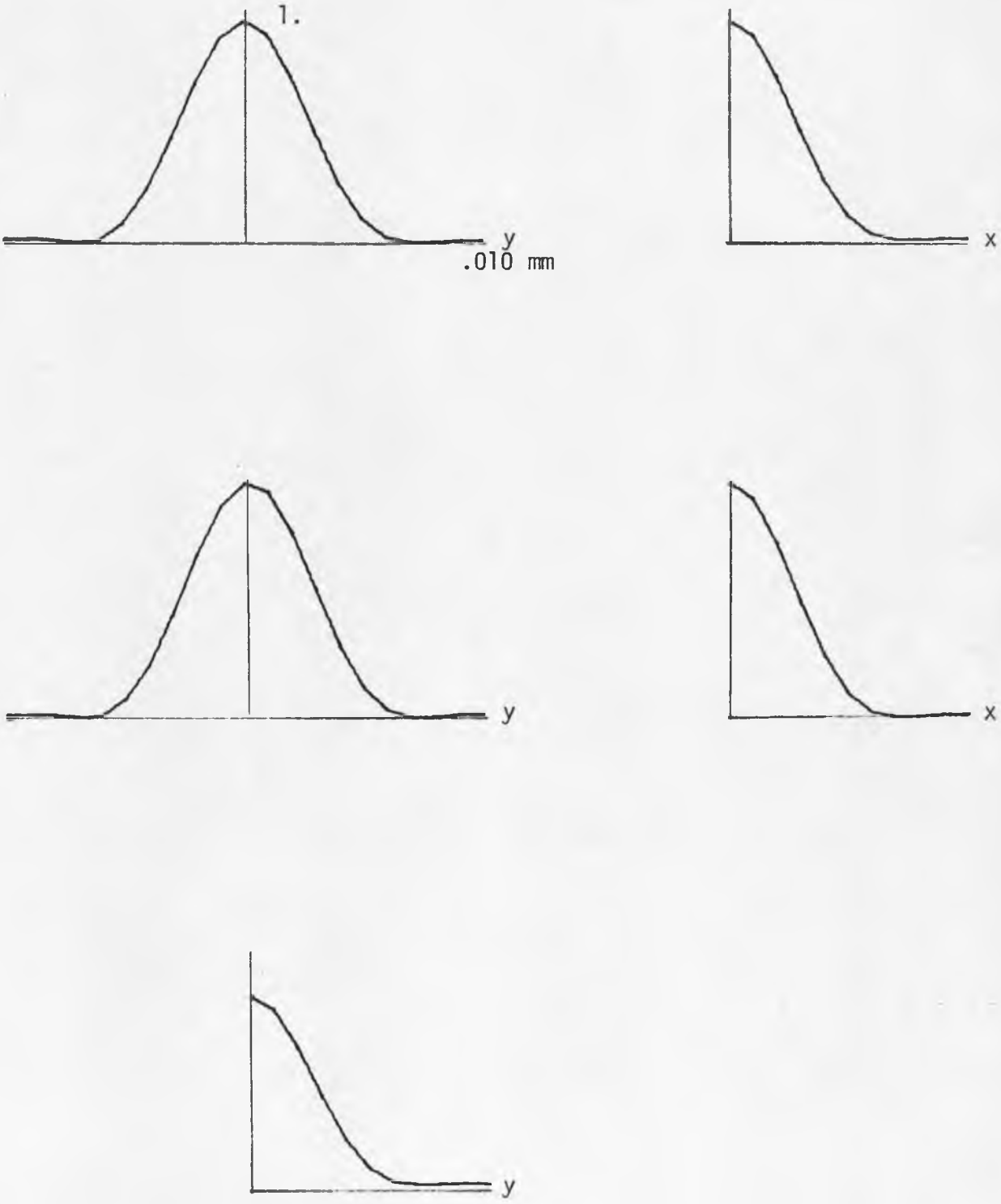

Figure 3.6. PSF's of the Unequal Focal Length Lenses, F9.1.

calls for both sets of conjugates to involve infinite distances in the single FTL, the approach to the design could not be fully automatic.

According to third order aberration theory for a thin lens, conjugate shift has a significant effect on spherical aberration, but no effect on astigmatism. Therefore, it seems reasonable to begin with the correction of spherical aberration as the most important consideration. Because the input format is so much larger than the Fourier transform diameter in this case, the optimization should proceed from the input end of the lens. Considering two identical asymmetric lenses, we see that in one direction the input diameter and focal length determine the f-ratio, and that spatial frequency determines the field angle. On the other side of the hologram, f-ratio is determined by hologram size and field angle by f-ratio of the first lens. We design the lens in one direction, then check the performance in the other. This will tell us how well the lens will mate with an identical lens in the correlator.

The design was initiated from a four element photographic objective. The stop was kept in the paraxial front focal plane with a paraxial chief ray angle solve on the last glass surface. The defect function was identical to that used for the optimization of symmetric triplets. After convergence of the optimization on a version of ACCOS, the lens was set up in the opposite direction with appropriate field angle and stop diameter alterations. A successful ray trace indicated that the lens would work in the correlator configuration.

To evaluate the lens in the imaging configuration, the input was placed at the paraxial front focal plane. The hologram was placed at

the focus chosen in the optimization as a FTL. An identical four element lens was placed symmetrically about the hologram plane. The final image plane was then chosen by the defect function. It is inside the paraxial focus due to some undercorrected field curvature. We could easily make the values of 154.921 and 154.7 converge to a common value by moving the input plane towards the first lens. Stop location has a weak effect on performance in the FTL configuration, so the value of 140.184 as the best focal distance would not change appreciably during this adjustment.

Table 3.3 contains a description of the lens, and Figures 3.7 and 3.8 demonstrate its performance in the correlator. It is essentially aberration free at all field positions.

Table 3.3. Asymmetric Lens in Imaging Configuration.

Radius (mm)	Thickness (mm)	Index at 632.8 nm
	154.921	Air
197.9414	18.	1.6138
-844.1525	1.17	Air
105.604	44.6	1.6138
170.7815	10.56	Air
-362.8605	4.7	1.72
78.5885	44.6	Air
311.4411	18.8	1.6138
-119.8658	140.184	Air
Stop	140.184	Air
119.8658	18.8	1.6138
-311.4411	44.6	Air
-78.5885	4.7	1.72
362.8605	10.56	Air
-170.7815	44.6	1.6138
-105.604	1.17	Air
844.1525	18.	1.6138
-197.9414	154.7	Air

EFL at 632.8 nm = 233.7738 mm
Paraxial front focal distance = 154.9208 mm
Paraxial back focal distance = 140.1955 mm
Airy disk radius = .020 mm

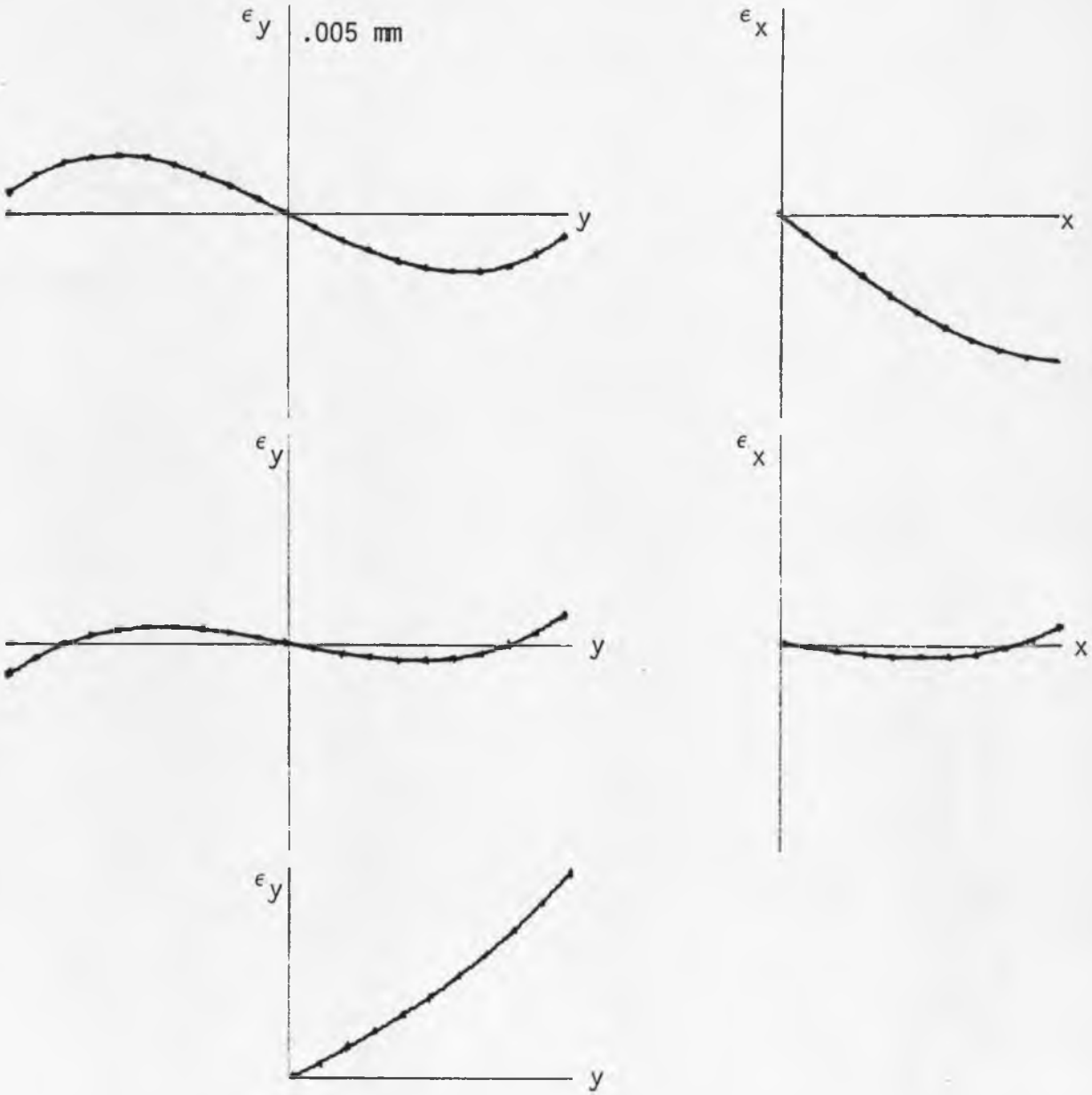

Figure 3.7. Ray Fans for Asymmetric Lenses in Imaging Configuration.

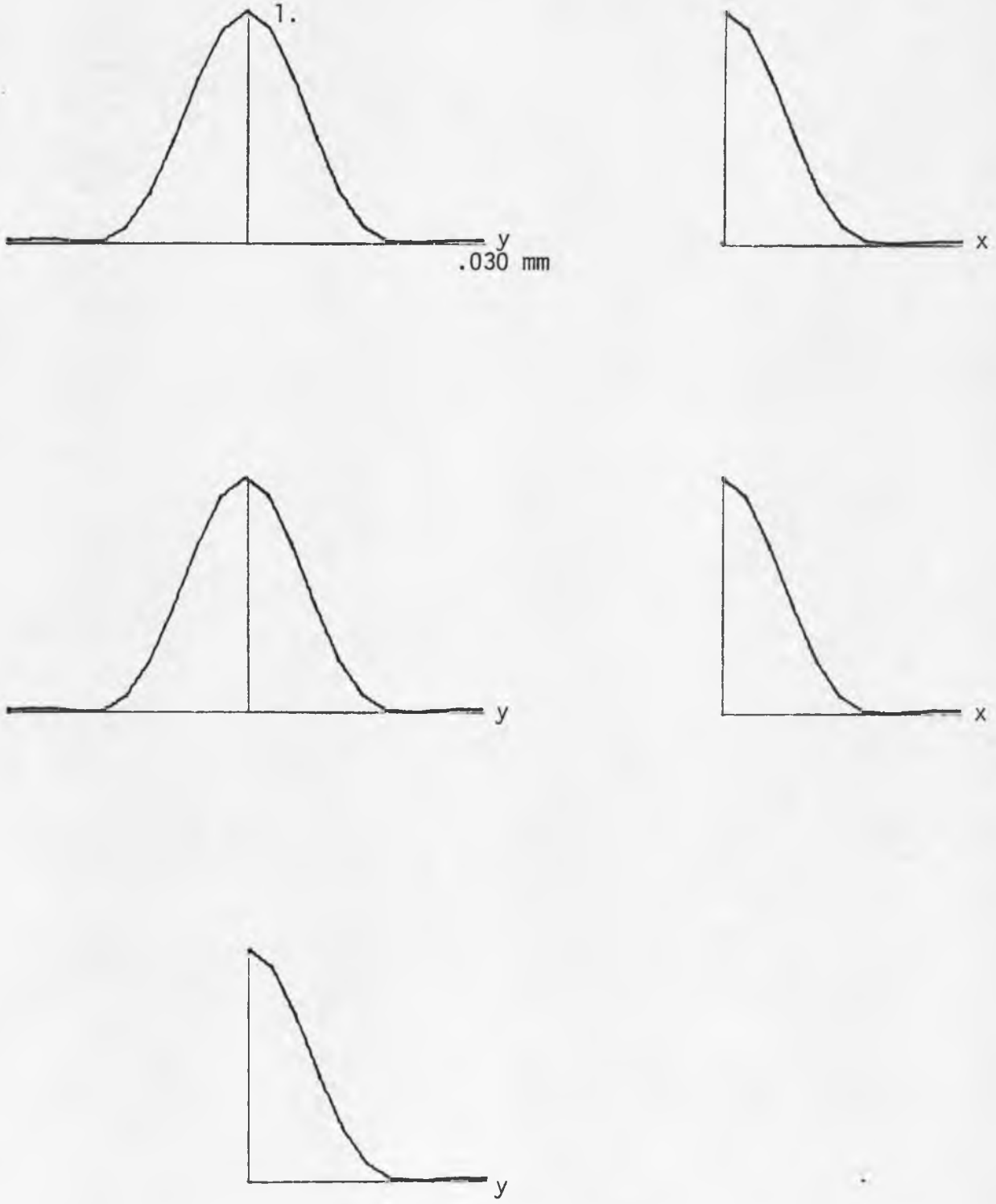

Figure 3.8. PSF's of the Asymmetric Lenses, F26.

CHAPTER 4

THE MULTIWAVELENGTH PROBLEM

In employing a lens for a FTL, the question of the lens's wavelength versatility sometimes arises. There can be reasons to change wavelengths for spectral sensitivity of the film or of the autocorrelation detector, or for laser stability characteristics.

Paraxial Properties

There are a number of new facets to be considered in moving to the design of a lens for several wavelengths. Figure 4.1 shows a transparency and a singlet FTL being used at three wavelengths. The shortest wavelength is depicted in the topmost lens. The focal length increases by 5% between the configurations. (Glasses have lower indices of refraction with increasing λ in the visible.) First the transparency is moved to the left and the focal plane to the right because of the increased focal length. Also, θ_{max} increases. (For this diagram, the wavelength ratio between levels is 1.25.) The increase in clear aperture at the lens is proportional to the product of these effects.

Figure 4.1 shows a lens with f-ratio 3.3 at the short wavelength and with θ_{max} equal to 0.1. This is a low F number, large field angle FTL. The values for the field angles were chosen to make the differences in the diagrams more apparent. However, the changes in focal length and field angle are representative of what is seen in changing from blue to red illumination. Thus, it is not unreasonable to allow

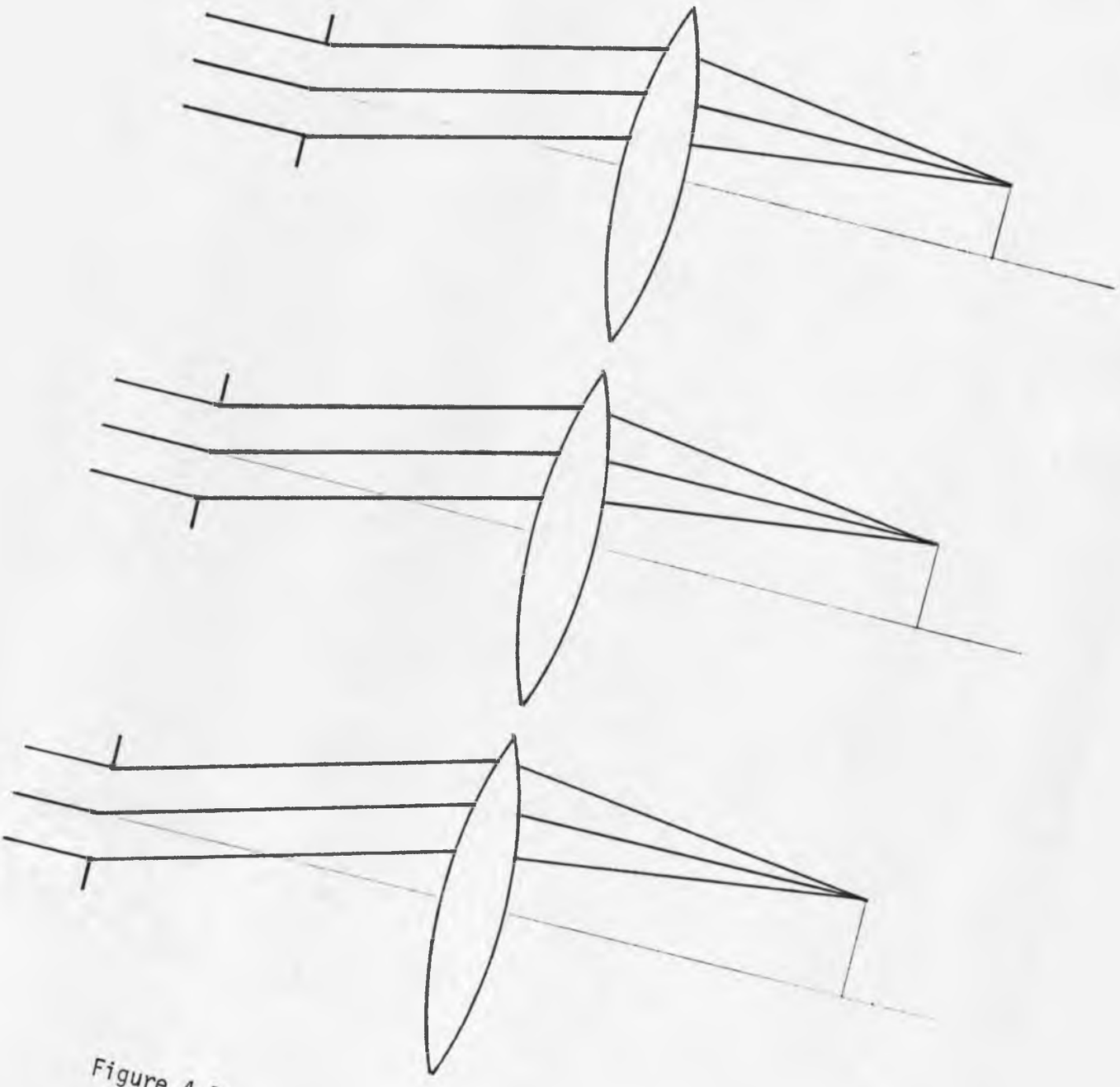

Figure 4.1. Increasing Illuminating Wavelength.

for chromatic variation of the transparency-to-lens distance and back focal distance (axial color). Typically, the change would be less than a few centimeters. For a multielement lens, we will require that the element spacings remain fixed and that the input and focus locations be symmetric about the lens for all wavelengths. We shall allow a change in the focal length with color (lateral color) so long as the change is within practical limits.

Optimization

There are three lenses and their evaluations presented in this chapter. In the first, it is assumed that the design field angle is independent of wavelength. It can be that θ_{max} at the longest wavelength is used as the design field angle, or that the maximum spatial frequency of the input is lower for the longer wavelengths. In this first lens, we also assume that two glasses with different dispersion values are needed to cope with color correction at widely separated wavelengths. The starting design is Steel's (1974) well-corrected triplet. The main result of the process is the demonstration that automatic optimization at two wavelengths without achromatization can be done with a ray defined defect function. (See Appendix D for card images to implement the ACCOS V defection function.) The lens is described in Table 4.1. Figures 4.2 through 4.5 give an evaluation of the lens.

In the second lens, only one glass type was allowed. The negative element of the first lens was given the same index and dispersion as the positive elements. Also, new curvatures for the negative element were calculated to preserve the focal length and back focal distance at

Table 4.1. Multiple Wavelength Lens.

Radius (mm)	Thickness (mm)	Glass Type
	10^{10}	Air
Stop	Red 430.8115 Blue 421.1499	Air
240.20176	12.5	BaK1
-932.95894	48.68299	Air
-242.03726	8.	Bk7
242.03726	48.68299	Air
932.95894	12.5	BaK1
-240.20176	Red 430.8115 Blue 421.1499	Air

Input format diameter = 40 mm

Semifield angle = $\tan^{-1}$ .04 (63 lp/mm at 632.8 nm
82 lp/mm at 488 nm)

EFL at 632.8 nm = 502.286321 mm

Paraxial back focal distance = 431.049247 mm

Real chief ray height at best focus = 20.07449 mm

fsinθ = 20.07540 mm

EFL at 488.0 nm = 492.841963 mm

Paraxial back focal distance - 421.460506 mm

Real chief ray height at best focus = 19.69553 mm

fsinθ = 19.69793 mm

Airy disk radii: at 488 nm = .0074 mm
at 632.8 nm = .0097 mm

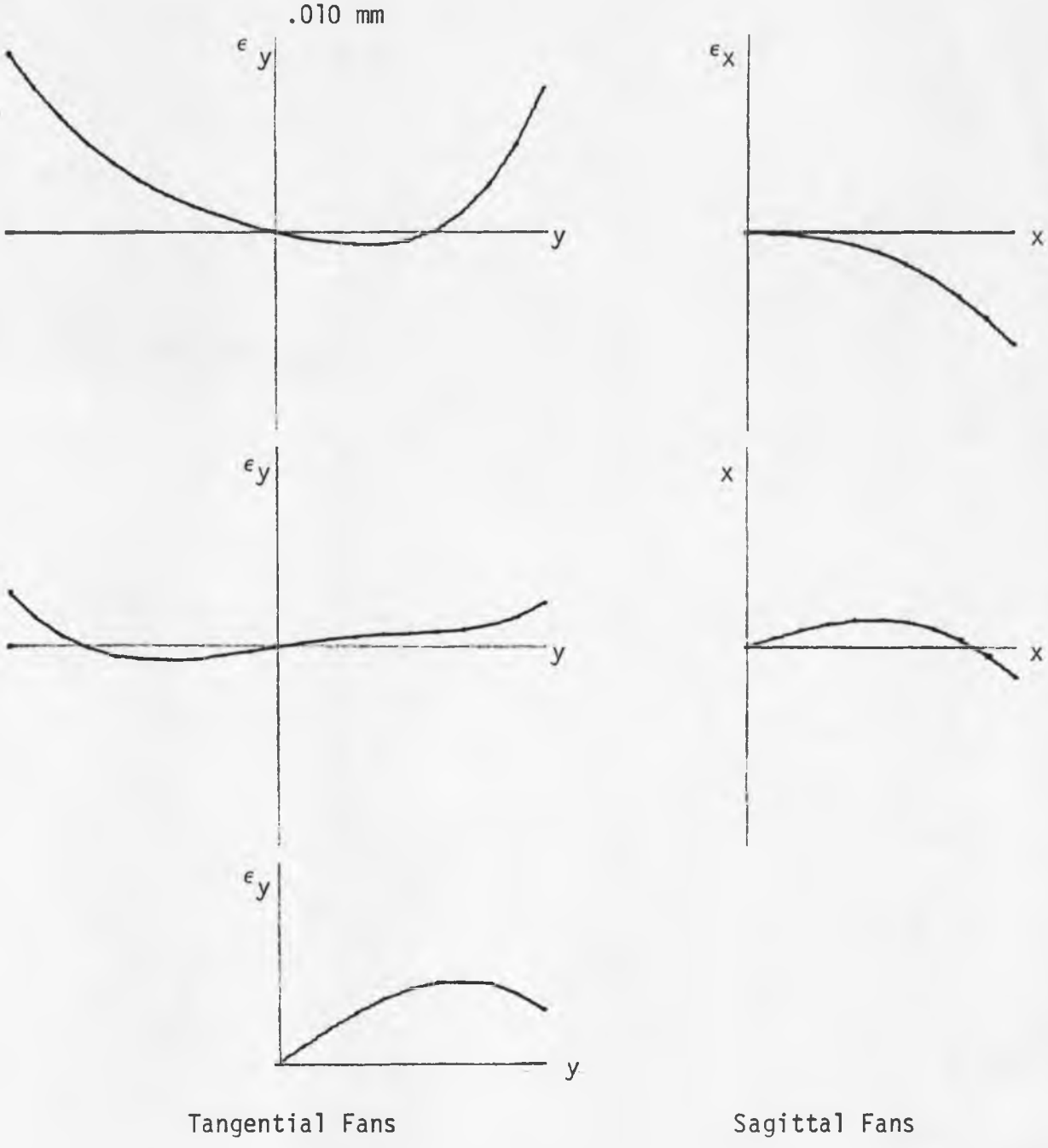

Tangential Fans

Sagittal Fans

Figure 4.2. Ray Fans for Multiple Wavelength Lens, Red.

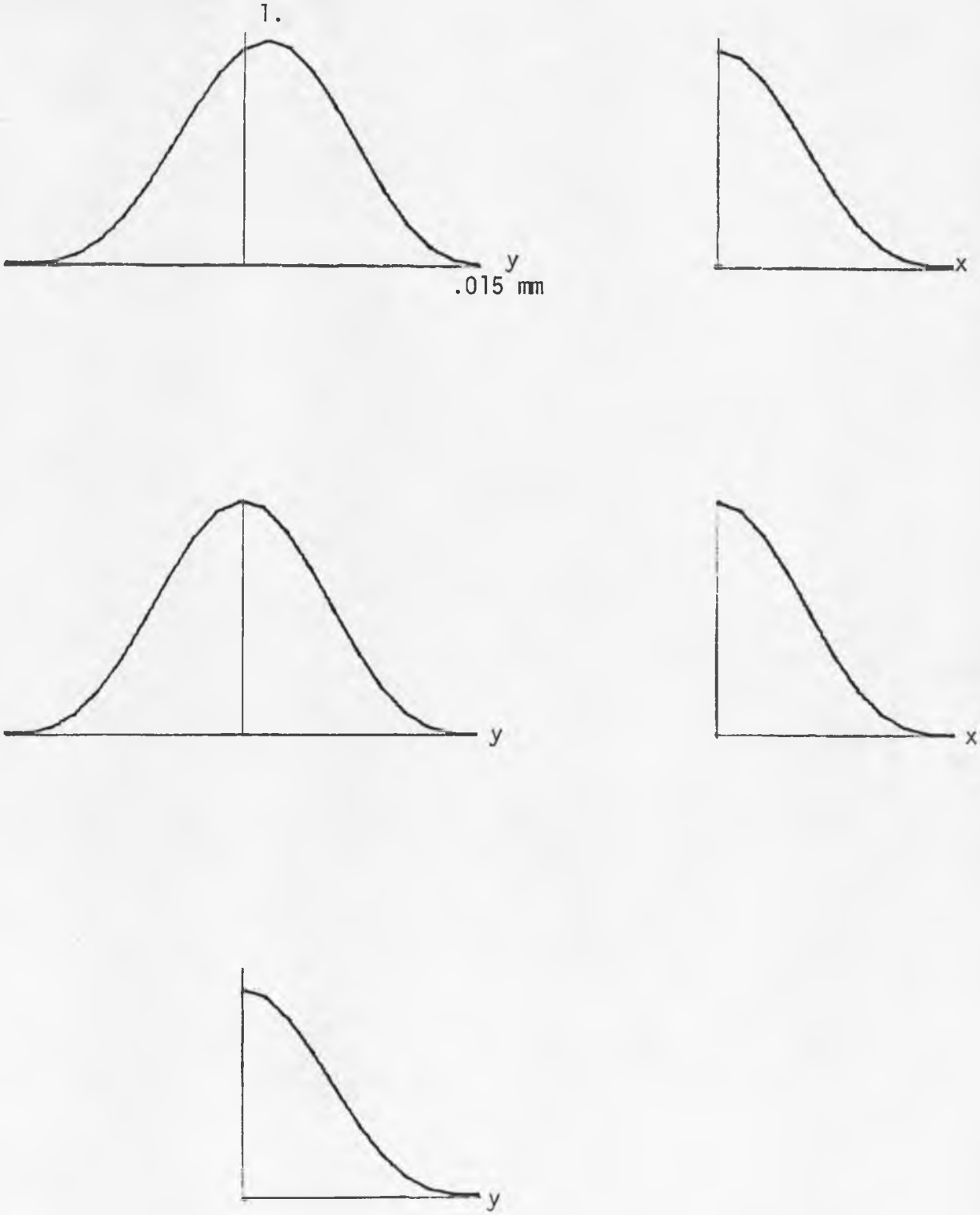

Figure 4.3. PSF's of Multiple Wavelength Lens, Red.

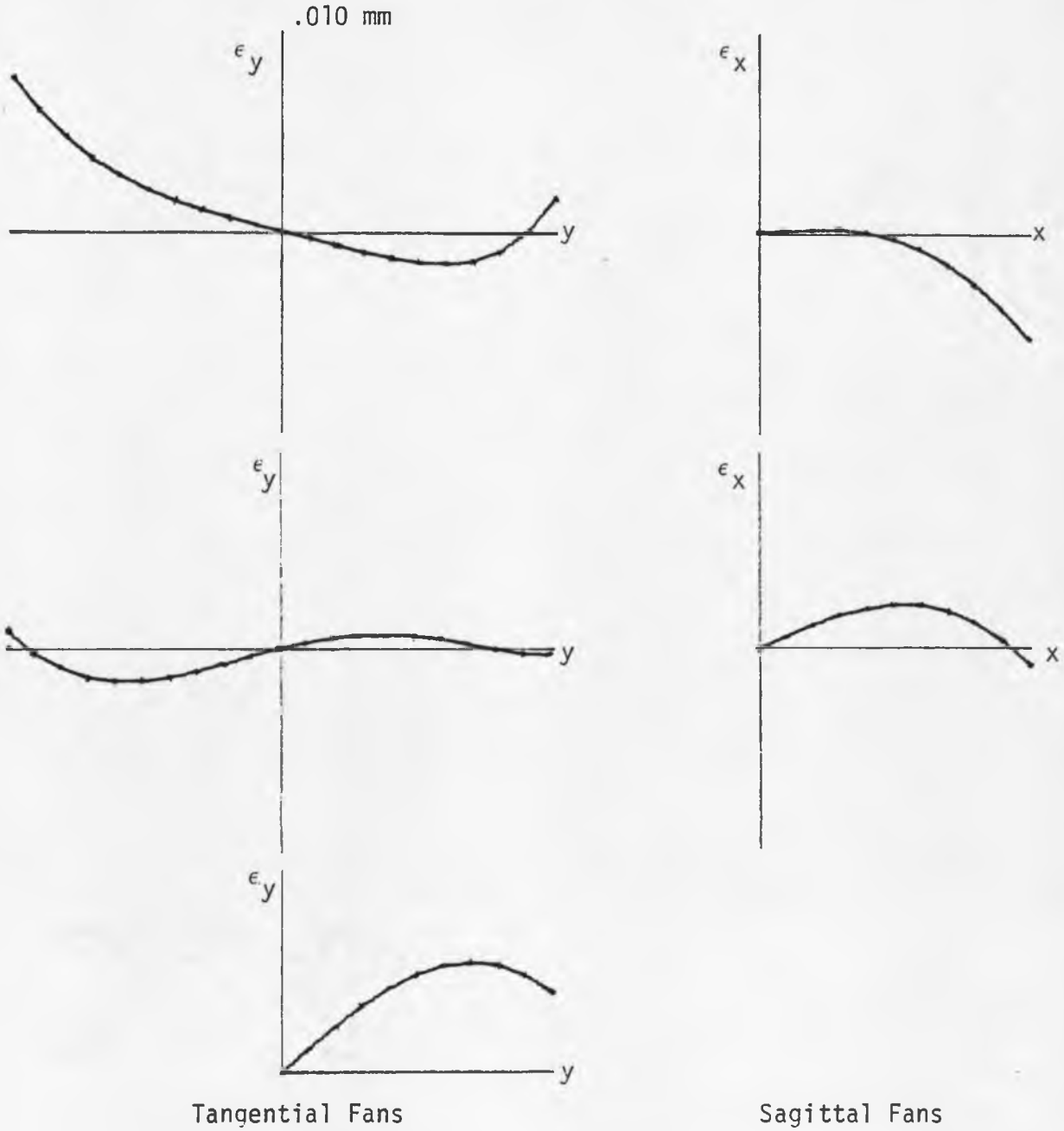

Figure 4.4. Ray Fans for Multiple Wavelength Lens, Blue.

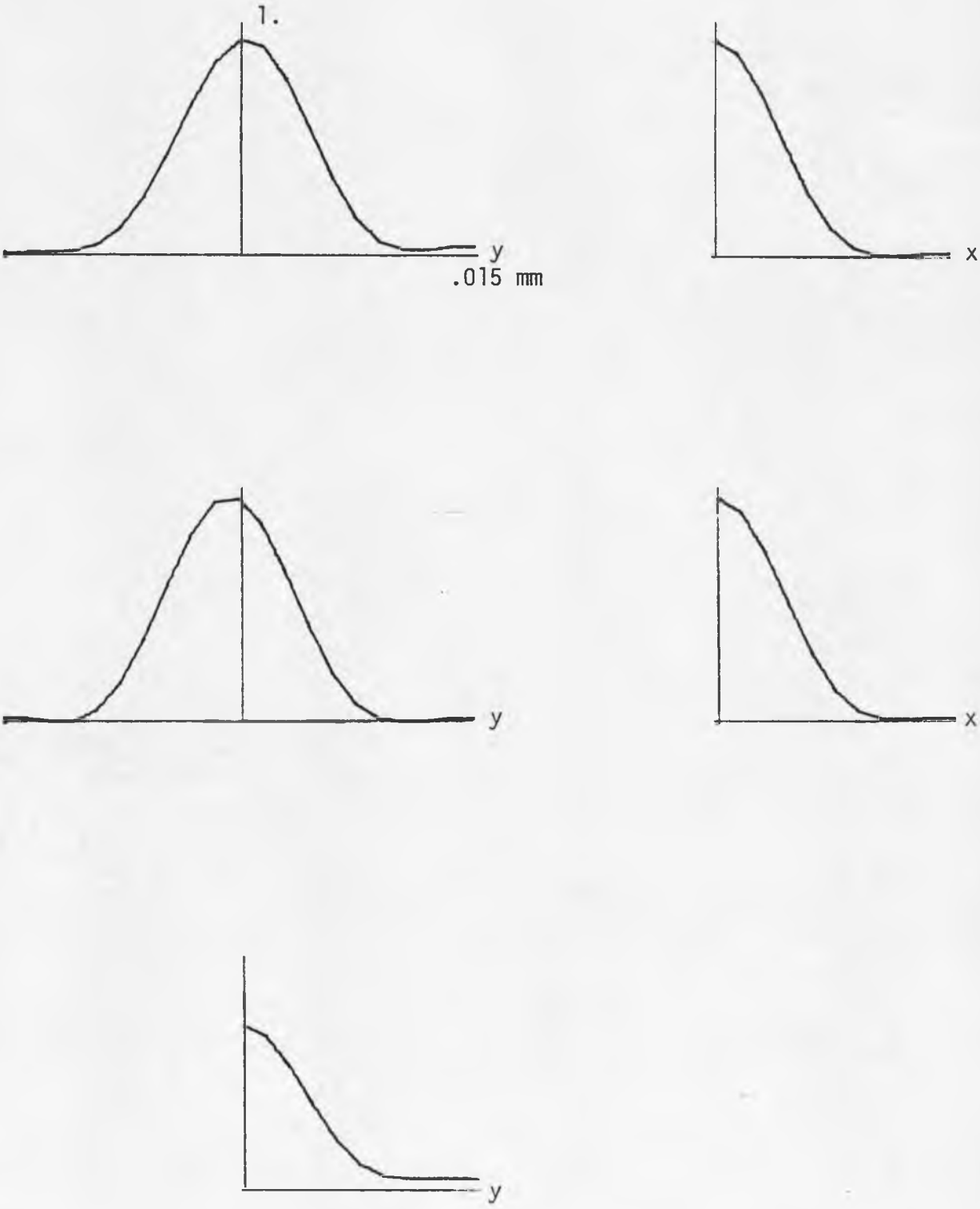

Figure 4.5. PSF's of Multiple Wavelength Lens, Blue.

one wavelength. The index and dispersion were variables in the optimization, but all elements have the same values for index and dispersion. After several optimization passes, a glass type with dispersion and index close go those of the optimized glass was selected from the Schott glass table. Several more passes were then made with only air thicknesses and element curvatures as variable. The optimization quickly converged to the values given in Table 4.2. Evaluations are given in Figures 4.6 through 4.9.

The third lens considers another facet of the problem. The defect function is so constructed that the design field angle is the maximum angle of diffraction for red light. The stop position is allowed to be at different locations for red light and for blue light, as in the first two cases, but now the design field angle for blue is smaller than that for red in direct proportion to the ratio of wavelengths. This defect function requires an addition of two card images to the defect function of Appendix D. Table 4.3 describes the lens. Evaluations are given in Figures 4.10 through 4.13.

We can make a comparison of the three lenses to see how much each consideration affects the final design and the performance. The fractional field heights are 0, .7, and 1 in all three lens evaluations. In doing this, note that the maximum field heights for red and blue are the same in the evaluation of the first two lenses, but that the actual field heights are different for the two colors in the evaluation of the third lens. (The field height is 20 mm for red and 15.2 mm for blue in the third lens.)

Table 4.2. Single Glass Lens.

Radius (mm)	Thickness (mm)	Glass Type
	10^{10}	Air
Stop	Red 447.6051 Blue 437.4584	Air
241.33766	12.5	BaF6
-904.13521	40.55215	Air
-262.65326	8.	BaF6
262.65326	40.55215	Air
904.13521	12.5	BaF6
-241.33766	Red 447.6051 Blue 437.4584	Air

Input format diameter = 40 mm

Semifield angle = $\tan^{-1}$ .04 (63 lp/mm at 632.8 nm
82 lp/mm at 488 nm)

EFL at 632.8 nm = 507.6387 mm

Paraxial back focal distance = 447.8870 mm

Real chief ray height at best focus = 20.2876 mm

fsinθ = 20.2893 mm

EFL at 488 nm = 497.6150 mm

Paraxial back focal distance = 437.7658 mm

Real chief ray height at best focus = 19.8866 mm

fsinθ = 19.8887 mm

Airy disk radii: at 488 nm = .0074 mm
at 632.8 nm = .0098 mm

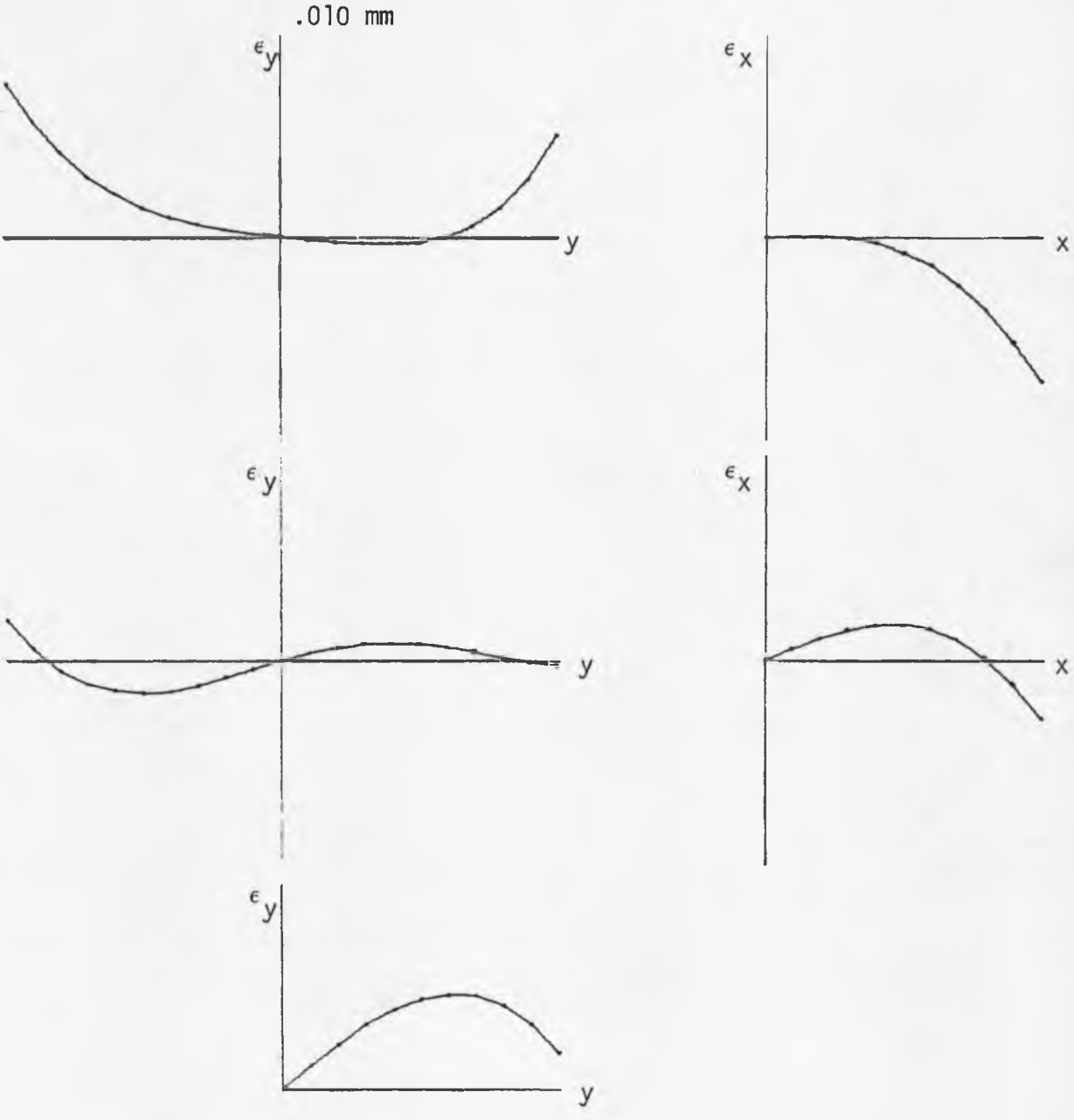

Figure 4.6. Ray Fans for Single Glass Multiple Wavelength Lens, Red.

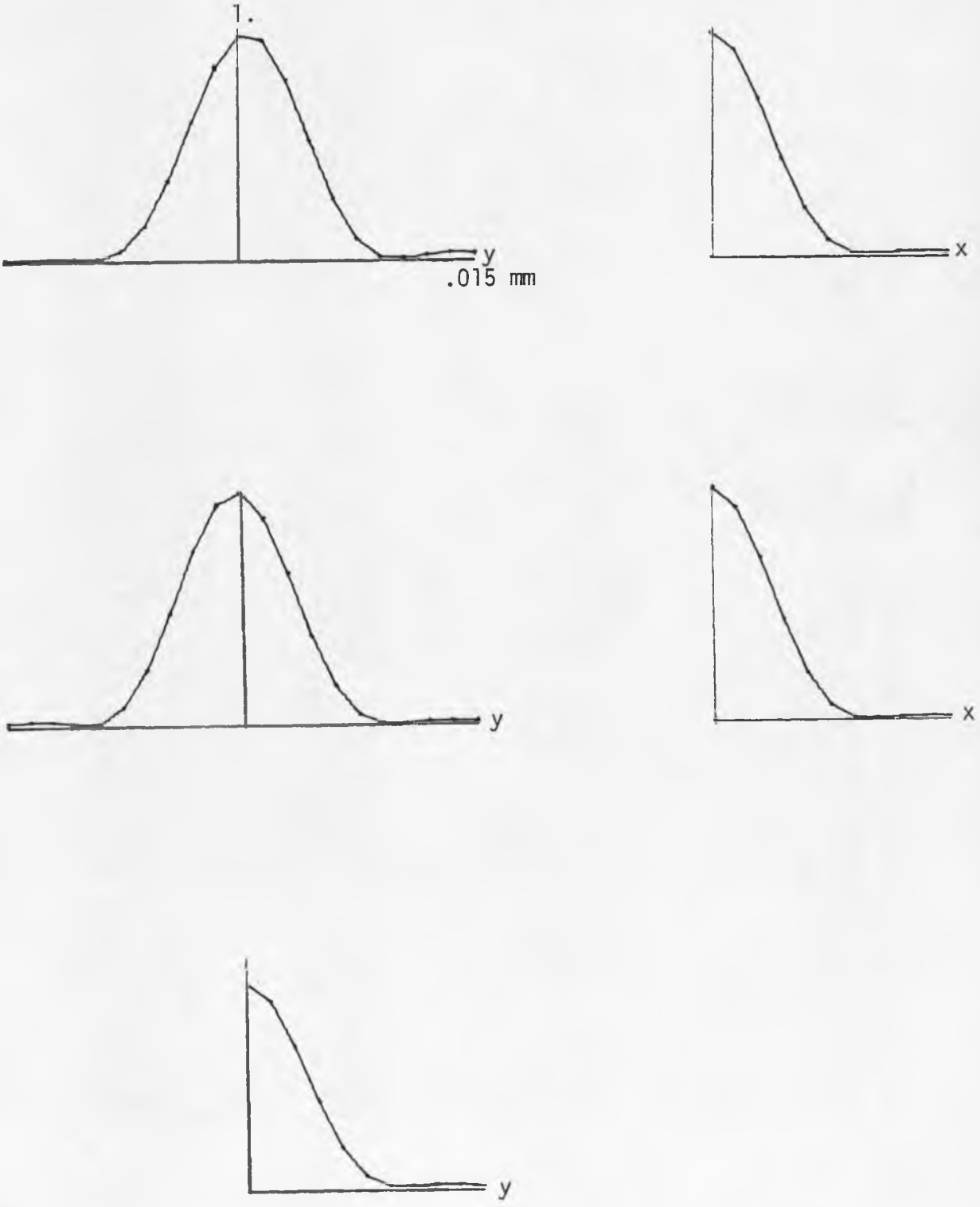

Figure 4.7. PSF's of Single Glass Multiple Wavelength Lens, Red.

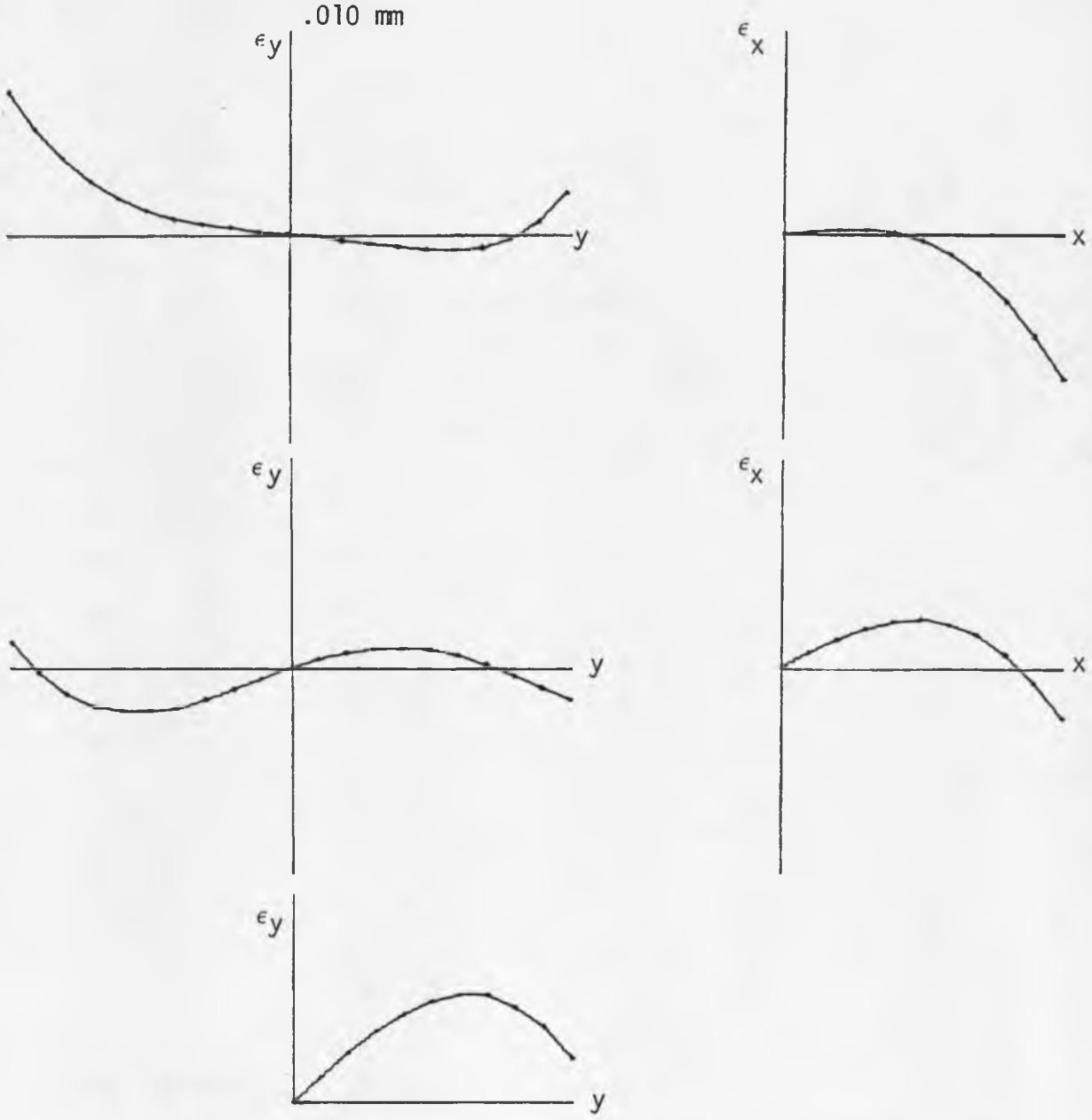

Figure 4.8. Ray Fans for Single Glass Multiple Wavelength Lens, Blue.

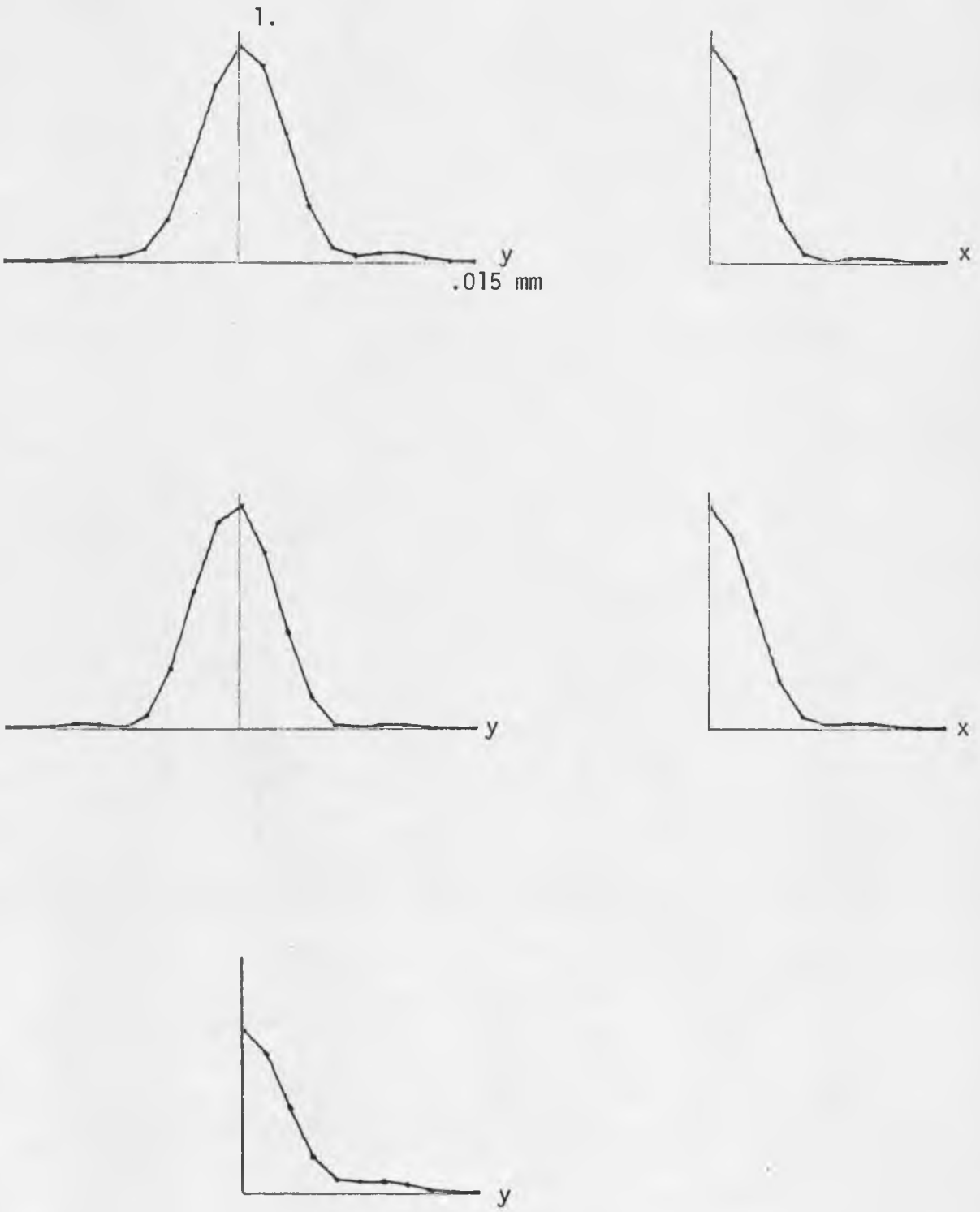

Figure 4.9. PSF's of Single Glass Multiple Wavelength Lens, Blue.

Table 4.3. Constant Spatial Frequency Lens.

Radius (mm)	Thickness (mm)	Glass Type
	10^{10}	Air
Stop	Red 447.36808 Blue 437.52814	Air
239.25847	12.5	BaF6
-916.89907	35.75243	Air
-264.81681	8.	BaF6
264.81681	35.75243	Air
916.89907	12.5	BaF6
-239.25847	Red 447.36808 Blue 437.52814	

Input format diameter = 40 mm

Spatial frequency: 63 lp/mm (field angle = $\tan^{-1}$ .04 in red and $\tan^{-1}$ .031 in blue)

EFL at 632.8 nm = 500.887477 mm

Paraxial back focal distance = 447.641605 mm

Real chief ray height at best focus = 20.01771 mm

fsinθ = 20.01949 mm

EFL at 488 nm = 491.080889 mm

Paraxial back focal distance = 437.775036 mm

Real chief ray height at best focus = 15.21514 mm

fsinθ = 15.216198 mm

Airy disk radii: at 488 nm = .0074 mm
at 632.8 nm = .0098mm

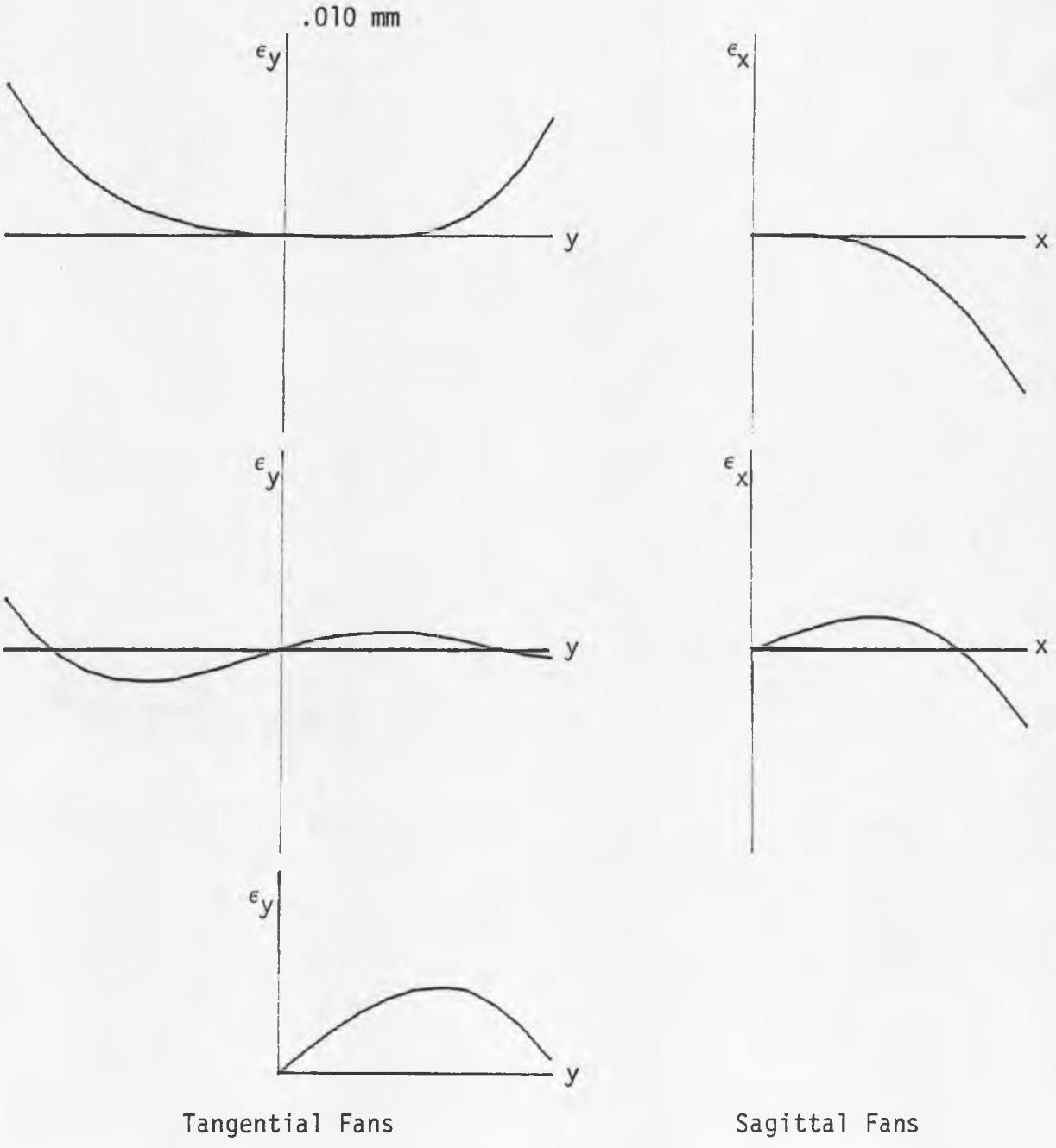

Figure 4.10. Ray Fans for Constant Spatial Frequency Lens, Red.

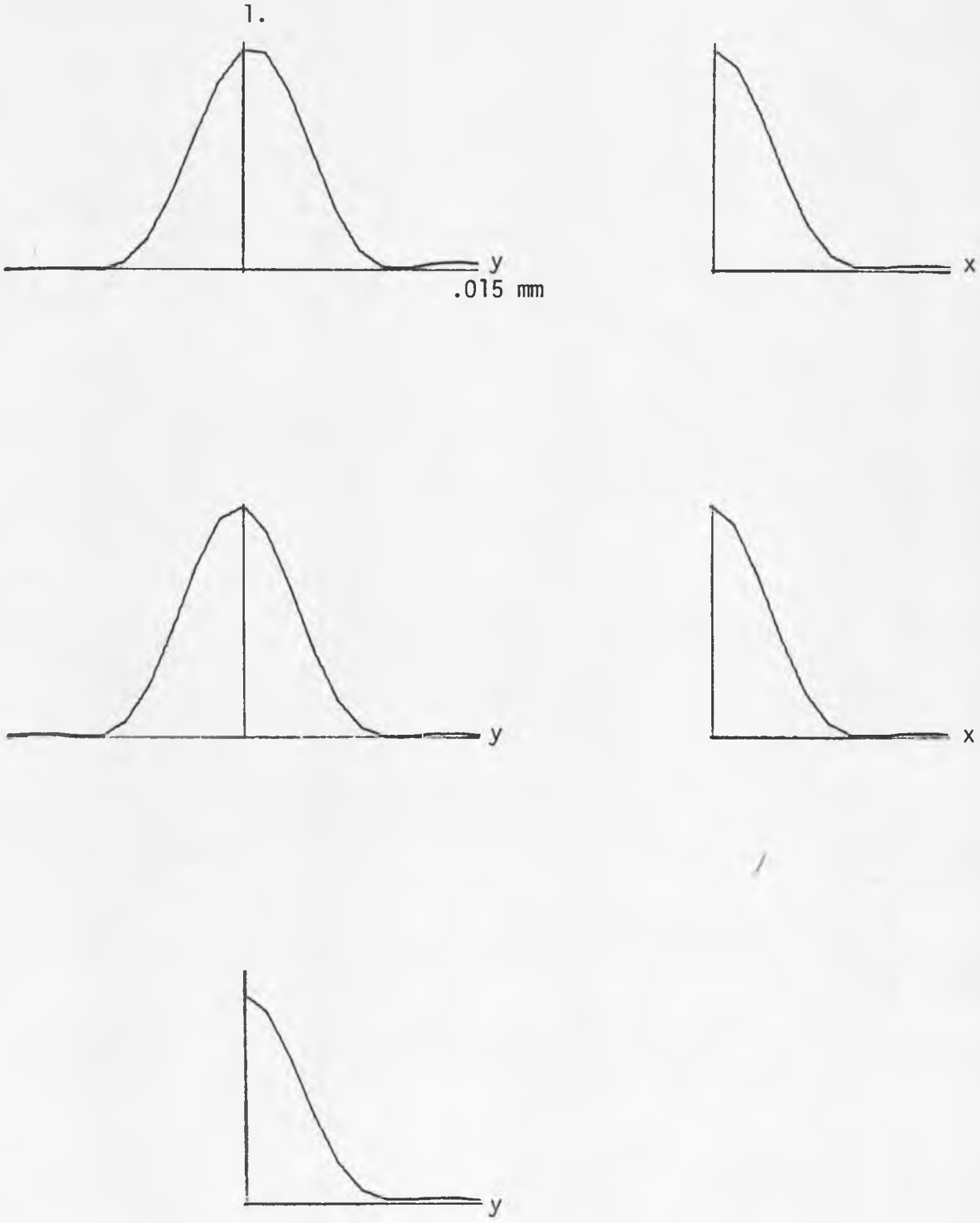

Figure 4.11. PSF's of Constant Spatial Frequency Lens, Red.

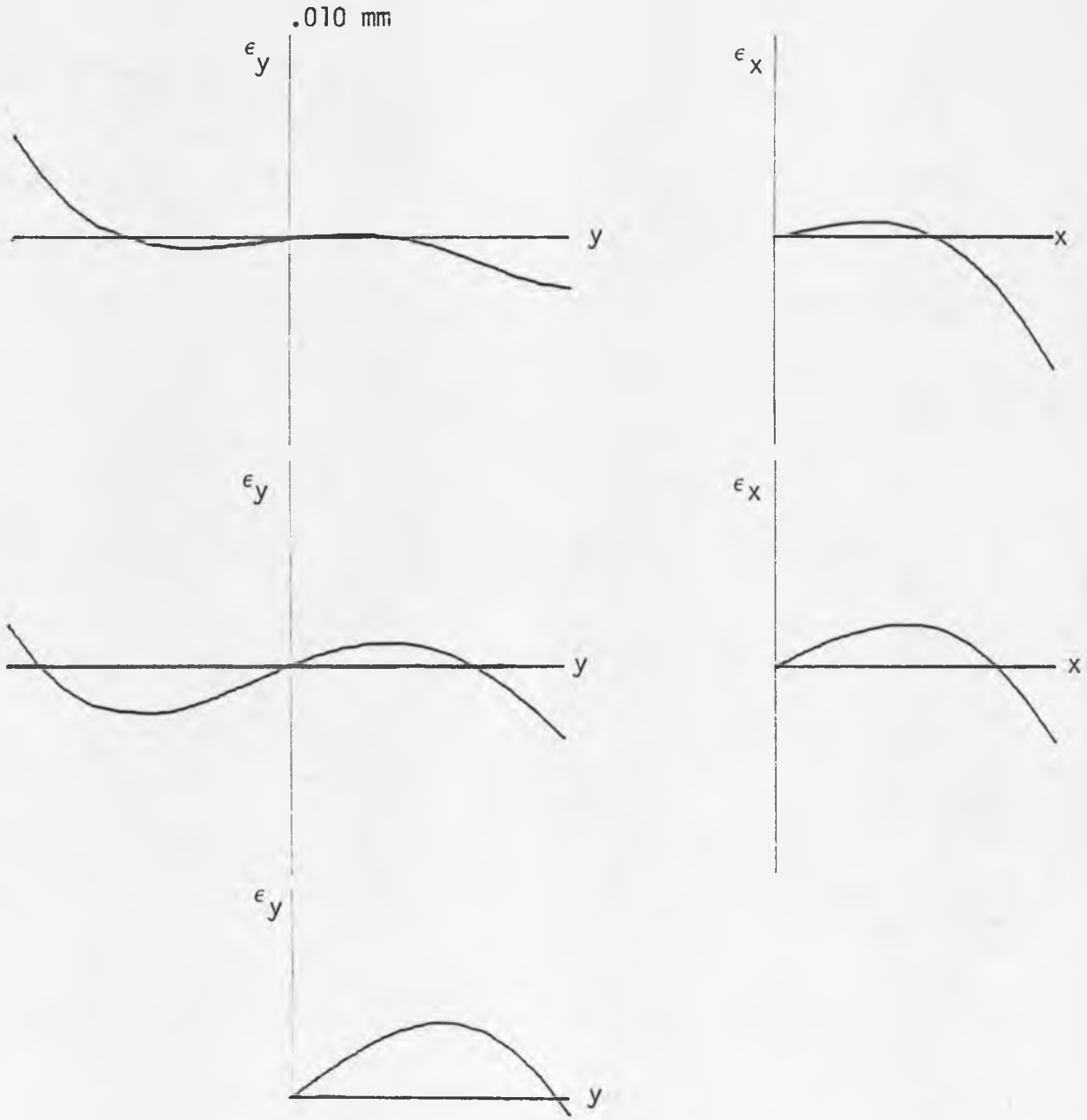

Figure 4.12. Ray Fans for Constant Spatial Frequency Lens, Blue.

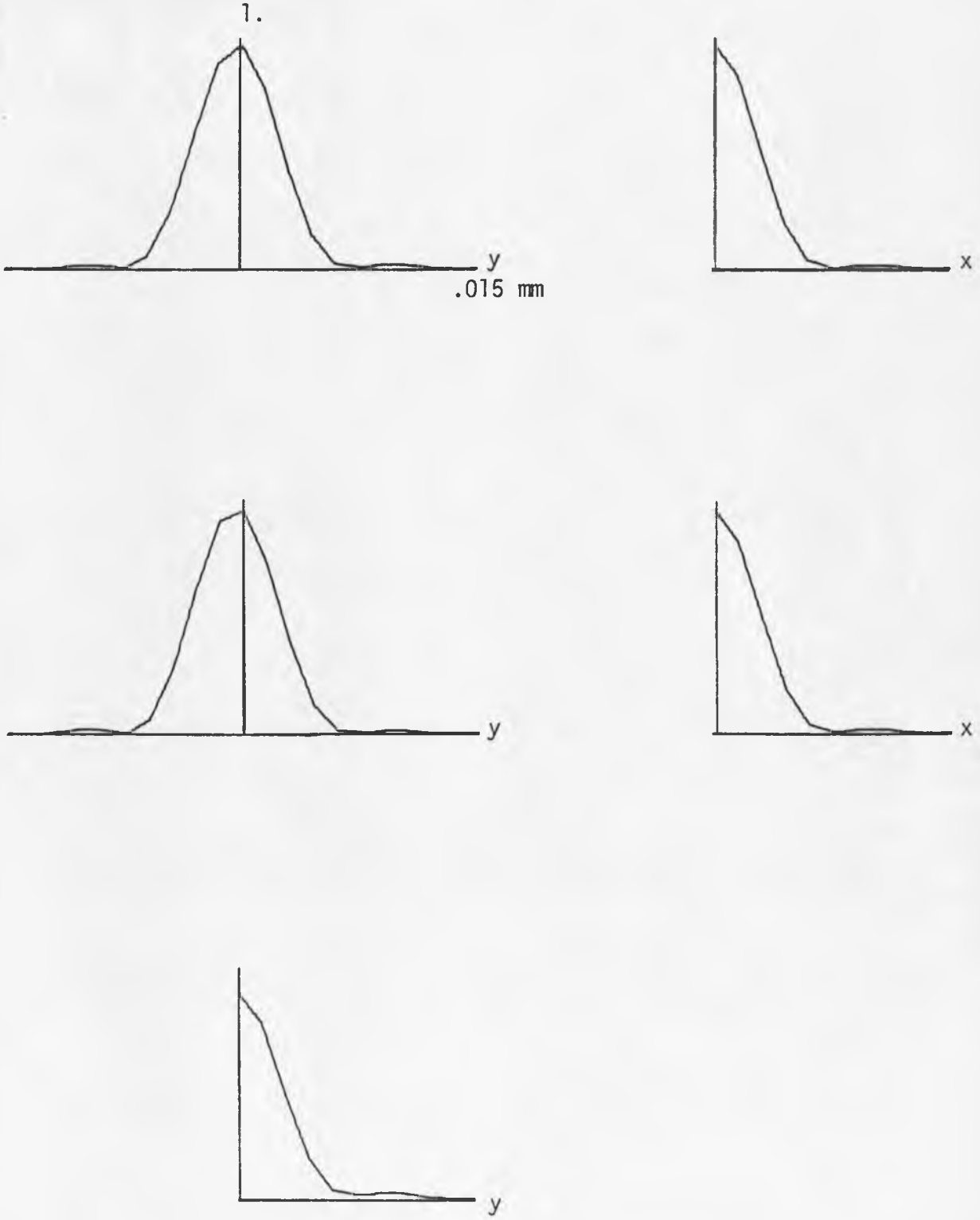

Figure 4.13. PSF's of Constant Spatial Frequency Lens, Blue.

Conclusions

Wynne (1974a) and Steel (1974) have both discussed the use of a FTL at several wavelengths. Blandford's (1970) comment was that a lens designed for one wavelength would not have well-corrected monochromatic aberrations at another wavelength if there were a large longitudinal chromatic aberration. Wynne designed several singlets which demonstrated that the aberration correction did not change quickly with wavelength. Steel designed a triplet with higher numerical aperture and larger field angle than Wynne's lenses. Steel commented that "it does not appear to be possible to correct a simple reversible triplet for all other aberrations when each component is a single lens made of a common glass; Blandford's theory confirms this" (1974, p. 36). Although it may not be possible to correct the Seidel aberrations with one glass, we see that balancing of aberrations can be accomplished in such a way that the design is essentially aberration free at a plane inside the paraxial focus. Figures 4.7, 4.9, 4.11, and 4.13 show that the wavefront is nearly spherical, even when only one glass type is used. The only noteworthy difference in the aberration correction for red and for blue is shown in the upper left-hand portion of Figure 4.10. In the red illumination, the necessity for a larger clear aperture at the lens leads to the introduction of a small amount of coma, especially at the maximum angle of diffraction in the red.

Structurally, the three lenses differ mostly in the physical extent of the glass elements. They are all nominally of 500 mm focal length. The difference between the red focal length and the blue focal

length is about one centimeter for all three lenses. The back focal distances changed by only 4% amongst the three lenses. It is the air spacing between elements that experienced the greatest change, differing by 25% between Table 4.1 and Table 4.3.

APPENDIX A

METHODS FOR STUDYING OPTICAL PROCESSORS

There are numerous configurations for the matched filter correlator. We will consider the Fresnel-Kirchhoff diffraction integral approach to describe the salient features of three configurations. In doing so, a methodology for examination of the general situation is developed. Cases may be treated on the basis of diffraction integrals alone, but it is shown that the quadratic phase factors may be handled more easily with the introduction of some ideas from geometrical optics.

Figure A.1 shows the five planes of interest for the derivations. For both the filter maker and for the correlator, the diffracting transparency lies at 1. A lens is placed at 2. The matched filter is at 3. See Goodman (1968, p. 171) for details on filter fabrication. In the correlator, a second lens is at 4. The detector is at 5. The distance D1 will be chosen equal to either f, the focal length of the lens, or zero, for these two values represent the extremes of the range of interest. We will assume the beam illuminating the transparency is collimated, for otherwise diffraction at 1 causes the wavefronts leaving 1 to be aberrated.

The distance between planes 2 and 3 equals the lenses' focal length, f, because we are considering collimated illumination at 1. For a spherical wavefront, the Fourier spectrum would lie at the plane of the image of the source of the illumination. The distance between

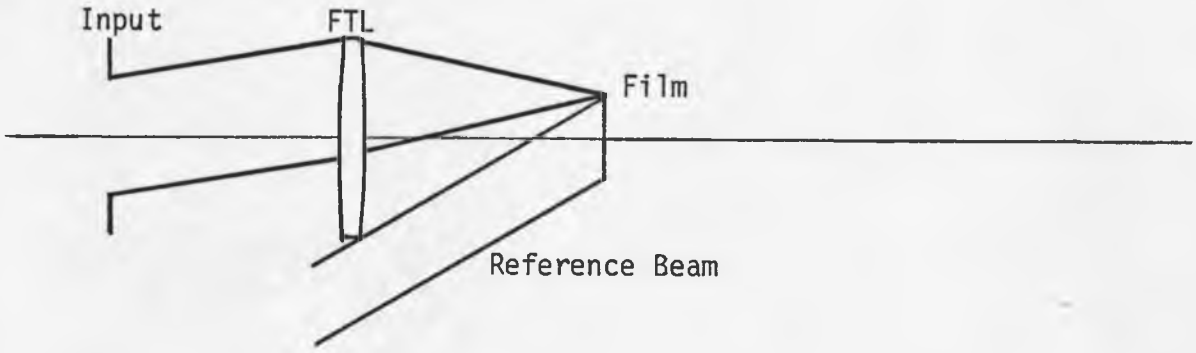

(a) Filter Maker.

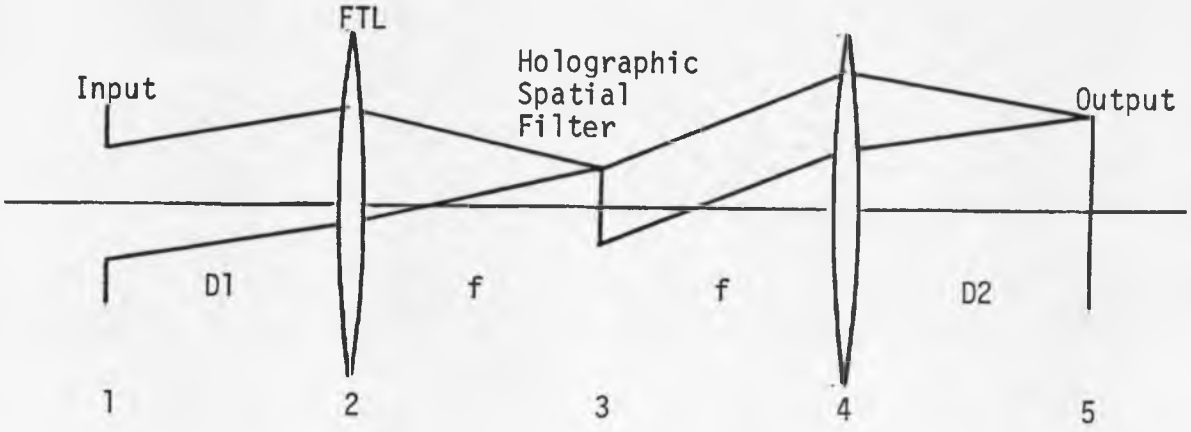

(b) Matched Filter Correlator.

Figure A.1. Matched Filter Correlator System.

planes 3 and 4 will always be equal to f for these examples. Further study for the allowable range of this distance would be interesting. The techniques developed here provide the tools to make the task reasonable. We do not attack the problem here because we saw no immediate gain in configuring a correlator in such a fashion. One obvious shortcoming of letting the distance approach zero is that requisite space for a prism and plate assembly (described later in this appendix) would be eliminated.

Lateral Shift of Correlator Input

The symbol u denotes electric field amplitude. A single variable, x, is used, though the problem is two dimensional. It is cumbersome to use two variables and provides no additional insight. To demonstrate the shift invariant feature of the correlator, the input transmittance is written $u_1(x_1 - x_0)$, viz., the matching signal is in the same plane as was the transparency used to prepare the matched filter, but it is shifted transversely.

The first case will be with D1 = D2 = f. Then with the electric field at 1 being $u_1(x_1 - x_0)$, we have at plane 2

$$u_2(x_2) = \int u_1(x_1 - x_0)\exp(i\pi(x_2 - x_1)^2/\lambda f)dx_1 \quad . \tag{A.1}$$

The amplitude transmittance of the lens at 2 is $\exp(-i\pi x_2^2/\lambda f)$. See Goodman (1968, p. 77). The field just to the right of a plane is indicated with a + sign. Thus,

$$u_2^+ = \exp(-i\pi x_2^2/\lambda f)u_2(x_2) \quad . \tag{A.2}$$

Propagating this field to 3, the plane of the matched filter, we have

$$u_3(x_3) = \iint u_1(x_1 - x_o)\exp(i\pi(x_2 - x_1)^2/\lambda f)$$

$$\cdot \exp(-i\pi x_2^2/\lambda f)\exp(i\pi(x_3 - x_2)^2/\lambda f)dx_1 dx_2 \quad . \qquad (A.3)$$

Collecting the terms in x_2, we have

$$\int \exp(i\pi(x_2^2 - 2x_1x_2 - x_2^2 - 2x_2x_3 + x_2^2)/\lambda f)dx_2 \quad , \qquad (A.4)$$

which is the Fourier transform of $\exp(i\pi x_2^2/\lambda f)$ with the frequency space variable $(x_1 + x_3)/\lambda f$. This is easily treated with the symbolism described by Cathey (1974, p. 372). The transformed function is $\exp(-i\pi(x_1 + x_3)^2/\lambda f)$ to within a multiplicative constant. This study is not concerned with irradiance levels, so such constants will not be carried. Substituting this expression back into Eq. (A.3), we get

$$u_3(x_3) = \int u_1(x_1 - x_o)\exp(i\pi(x_1^2 + x_3^2)/\lambda f)$$

$$\cdot \exp(-i\pi(x_1^2 + 2x_1x_3 + x_3^2)/\lambda f)dx_1$$

$$= \tilde{u}_1(x_3/\lambda f)\exp(-i2\pi x_o x_3/\lambda f) \quad , \qquad (A.5)$$

where the tilde indicates the Fourier transform of the function. Thus, the amplitude at plane 3 due to the diffraction at 1 equals the Fourier transform of the amplitude transmittance at 1. The linear phase term is introduced by moving the input to an off axis point in 1. This derivation describes the Fourier transforming property of a lens, achieved when we assume that the quadratic phase factor provides a complete description of the transmittance of the lens. The final expression for u_3

gives the amplitude at the lens's rear focal plane for the light passing through the transparency. If a coherent collimated beam is introduced at a reasonably small angle, θ, say less than 20°, a hologram of the Fourier transform can be formed at 3. Larger reference beam angles require greater spatial resolution of the film, and make the hologram's output more sensitive to the reconstruction beam angle. The need for an appreciable back focal distance in order to accommodate a reference beam is shown in Figure A.1(a). If photographic film records this interference pattern,

$$|u(x_3) + \exp(i2\pi\alpha x_3)|^2 \quad ,$$

where $\alpha \equiv \sin\theta/\lambda$ and is processed to yield an amplitude transmittance proportional to the irradiance in the pattern, the amplitude transmittance of the hologram produced is given by (we assume that $x_0 = 0$ in the filter maker, for the operator is free to choose the value for x_0 at that point)

$$t(x_3) = 1 + \tilde{u}_1(x_3/\lambda f)\tilde{u}_1^*(x_3/\lambda f) + \tilde{u}_1(x_3/\lambda f) \cdot \exp(-i2\pi\alpha x_3) + \tilde{u}_1^*(x_3/\lambda f)\exp(i2\pi\alpha x_3) \quad . \qquad (A.6)$$

Such a hologram is called a matched filter. Again, constants related to relative irradiances have been neglected for convenience.

Let the input to the correlator contain the signal from which the holographic filter was made. (In the correlator, the transmittance at 1 should rigorously be written $u(x_1) = u_1(x_1 - x_0) + u'(x_1)$, where $u'(x_1)$ describes the transmittance of all the other (nonmatching)

signals also residing on the input transparency. We shall ignore these signals in our calculations. Such signals can give rise to detectable irradiance levels at 5, and are called "false alarms." In our treatment, we will merely show how the terms from the matching signals interact. Locations of output at 5 from false alarms can be calculated by the same methods. One merely assumes that some part of a $u'(x_1)$ introduced on a transparency is like $u_1(x_1)$ and calculates the position for that signal. Unfortunately, the abbreviated treatment given here might be somewhat confusing. However, a treatment containing terms for several signals on one transparency, with one being the matching signal, leads to a plethora of integrals to consider. Hopefully, the presentation given here optimizes the relationship between clarity and completeness.) In the filter maker, a collimated beam illuminates 1, and a coherent collimated beam illuminates 3. In the correlator, a collimated beam illuminates 1, but only the Fourier transform amplitude falls on the matched filter at 3. Then the amplitude to the right of the filter is $u_3(x_3)\cdot t(x_3)$. Propagation of this amplitude to the plane of the lens at 4 yields

$$u_4(x_4) = \int u_3(x_3)t(x_3)\exp(i\pi(x_4 - x_3)^2/\lambda f)dx_3 \quad . \tag{A.7}$$

Multiplying this by the transmittance of the lens gives

$$u_4^+(x_4) = u_4(x_4)\exp(-i\pi x_4^2/\lambda f)$$

$$= \int \exp(i\pi x_3^2/\lambda f)\exp(-i2\pi x_3 x_4)[\tilde{u}_1 \exp(-i2\pi x_o x_3/\lambda f)$$

$$+ \tilde{u}_1\tilde{u}_1\tilde{u}_1^*\exp(-i2\pi x_o x_3/\lambda f) + \tilde{u}_1\tilde{u}_1\exp(-i2\pi\alpha x_3)$$

$$\cdot \exp(-i2\pi x_o x_3/\lambda f)\tilde{u}_1\tilde{u}_1^*\exp(i2\pi\alpha x_3)\exp(-i2\pi x_o x_3/\lambda f)] \quad . \tag{A.8}$$

Eq. (A.8) has but one quadratic phase factor. In accordance with Eq. (A.2), propagation a distance f beyond 4 will result in a Fourier transform multiplied by linear phase terms. (We temporarily return to using $t(x_3)$ rather than all the terms inside the square brackets.)

$$u_5(x_5) = \int\int \tilde{u}_1(x_3/\lambda f)\exp(-i2\pi x_o x_3/\lambda f)t(x_3)\exp(i\pi(x_3^2 - 2x_3x_4)/\lambda f)$$

$$\cdot \exp(i\pi(x_5 - x_4)^2/\lambda f)dx_3dx_4 \quad . \tag{A.9}$$

Collecting only the terms in x_4,

$$\int \exp(i\pi(x_4^2 - 2x_3x_4)/\lambda f)\exp(-i\pi x_4^2/\lambda f)\exp(i\pi(-2x_4x_5 + x_4^2)/\lambda f)dx_4$$

$$= \int \exp(i\pi x_4^2/\lambda f)\exp(-i2\pi(x_3 + x_5)x_4/\lambda f)dx_4 \quad , \tag{A.10}$$

which is the Fourier transform of $\exp(i\pi x_4^2/\lambda f)$ with transform variable $(x_3 + x_5)/\lambda f$. Substituting this last expression into the equation for $u_5(x_5)$, we obtain

$$u_5(x_5) = \int \tilde{u}_1(x_3/\lambda f)\exp(-i2\pi x_o x_3/\lambda f)t(x_3)\exp(-i2\pi x_3 x_5/\lambda f)dx_3 \quad ,$$

(A.11)

which is the Fourier transform of $\tilde{u}_1(x_3/\lambda f)\cdot\exp(-i2\pi x_o x_3/\lambda f)\cdot t(x_3)$ with transform variable $x_5/\lambda f$. Thus, the four terms of Eq. (A.6) result in these four terms at 5:

$$
\begin{aligned}
u_5(x_5) = {} & u_1(-x_5)*\delta(x_5 + x_o) && \text{Image} \\
& + u_1(-x_5)*u_1(-x_5)*u_1^*(-x_5)*\delta(x_5 + x_o) && \text{Triple Convolution} \\
& + u_1(-x_5)*u_1(-x_5)*\delta(x_5 + x_o + \alpha\lambda f) && \text{Self-Convolution} \\
& + u_1(-x_5)\star u_1(-x_5)*\delta(x_5 + x_o - \alpha\lambda f) && \text{Autocorrelation.}
\end{aligned}
\qquad (A.12)
$$

The term of greatest interest is the last, the autocorrelation. It lies at $x_5 = -x_o + \alpha\lambda f$. Similarly, the $\tilde{u}_1$ term in $t(x_3)$ results in a self-convolution at $x_5 = -x_o - \alpha\lambda f$. Thus, the two are positioned symmetrically about the image point $x_5 = -x_o$. From the linear appearance of x_o in this last equation for $u_5(x_5)$, we see that the correlator is indeed shift invariant. Note that we have assumed here that the impulse response of the system does not change with the location in plane 5. This is what the psf diagrams in Chapters 2, 3, and 4 confirm or disprove for the lenses considered in those chapters.

The choice of α is a free variable, within the limits of the ability of the film to record the fringe spacing. The terms at the output plane can be separated by choosing α properly. Goodman (1968, p. 176) presented some inequalities to describe the criteria for separating the terms. His treatment dealt only with axial signals, however. For

the case of an off-axis input to the correlator, all the output terms are shifted in direct proportion to the input's shift. An example will help clarify the relationships. Let us consider a correlator with the format and focal lengths described in Chapter 3. The lenses will be of equal focal lengths. The system is illuminated with helium neon laser light and a reference beam angle of 20° was used to form the spatial filter. We now have

$$\lambda = 6.328 \cdot 10^{-4} \text{ mm} \quad ,$$

$$\theta = 20° \quad ,$$

$$\alpha \equiv \sin\theta/\lambda = 540.5/\text{mm} \quad ,$$

$$\alpha\lambda f = 80.38 \text{ mm} \quad .$$

For a format radius of 18 mm, there will be an image of the input transparency with radius of 18 mm centered on the origin. Let us suppose the matching signal is introduced at x_0 = 15 mm and has a radius of 3 mm. The output plane contains the terms represented in Figure A.2 (among the others mentioned above). Within the image of the input is the image of the matching signal, of course. The other terms represented are the autocorrelation of the matching signal at

$$x_5 = -15 \text{ mm} + 80.38 \text{ mm} = 75.38 \text{ mm} \quad ,$$

and the self-convolution of the matching signal at

$$x_5 = -15 \text{ mm} - 80.38 \text{ mm} = -95.38 \text{ mm} \quad .$$

Autocorrelation of Matching Signal

Image of Input Format

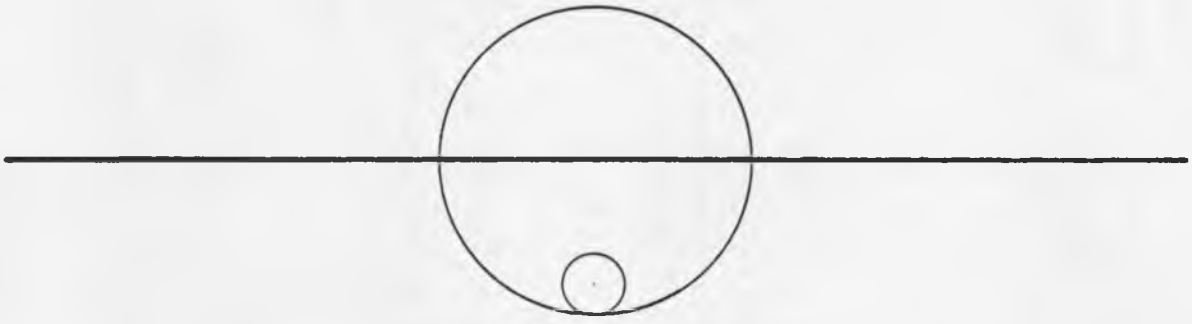

Image of Matching Signal

Self-convolution of Matching Signal

Figure A.2. Output Plane of Correlator.

With multiple inputs to the correlator on a single transparency, there are also a number of cross correlation terms. Several inequalities can be written, but the most pertinent is that for the relationship between the autocorrelation of the matching signal and the input format image, for the triple convolution is relatively weak. Let R_f be the radius of the format and R_s the radius of the matching signal. The limiting case is described by using a maximum value for x_o, for then the edge of the autocorrelation falls closest to the edge of the format image. For separation, it is necessary that

$$-x_o + \alpha\lambda f > R_f + 2R_s \tag{A.13}$$

However, x_o cannot exceed $R_f - R_s$ if the signal lies entirely within the input format. Therefore,

$$-(R_f - R_s) + \alpha\lambda f > R_f + 2R_s ,$$

or

$$\alpha\lambda f > 2R_f + R_s \tag{A.14}$$

A prism designed to deviate the beam exiting the filter for an on axis input to the correlator by an angle θ toward the axis will move the autocorrelation to the optical axis at the detector. The beam will still strike the last lens above the axis by an amount determined by the prism's distance from the matched filter plane. The incoming beam will be centered on the lens if a tilted plate to displace the beam is added to the assembly at a point behind the deviating prism and before the lens. An off axis match input results in a beam leaving the matched

filter at a small angle from the central ray for the on axis match. For the example above, the beam for the autocorrelation leaves the hologram at $\tan^{-1}(15/235)$ away from the beam for an on axis matched signal. This angle is 3.7°. The full angle for the configuration without the prism would be 20° + 3.7° = 23.7°. If the input were at x_o = -15 mm, the angle would be 20° - 3.7° = 16.3°. By installing a prism, the center of the angular spread is shifted to zero, greatly reducing the field angle requirements on the last lens. The inequality for separation in 5 is not altered. If no orientation search is required, the lens itself could be shifted and tilted, of course. If the filter is rotated for an orientation search, then the prism and plate assembly must also be rotated. The assembly must be carefully aligned with the reference beam in the filter maker, for otherwise the autocorrelation describes an arc on the detector rather than a small disk.

With the autocorrelation shifted to have a mean location at the intersection of the optical axis with plane 5, the geometrical optics for the system becomes identical to that for an afocal doubly telecentric imaging system without the hologram and the prism and plate assembly. Thus, we evaluate the aberration correction of the Vander Lugt correlator as described in Chapter 3 and Appendix C.

Longitudinal Shift of Correlator Input

We have just completed calculations for a transverse shift of the signal in the input plane. The next feature of interest is longitudinal movement of the input from the front focal plane of the first lens. As an extreme, we will make the calculations for a correlator

with plane 1 moved into coincidence with plane 2. (Moving the input away from 2 creates a requirement for a lens with larger aperture.) It is assumed that the matched filter was made just as in the previous case, with the transparency in the lens's front focal plane. The electric fields at the planes of the system are given by the integrals in Eqs. (A.15) through (A.21), with $x_o = 0$ for convenience.

$$u_2^+(x_2) = u_1(x_1)\exp(-i\pi x_2^2/\lambda f) \quad . \tag{A.15}$$

$$u_3(x_3) = \int u_2^+(x_2)\exp(i\pi(x_3 - x_4)^2/\lambda f)dx_2$$

$$= \tilde{u}_1(x_3/\lambda f)\exp(i\pi x_3^2/\lambda f) \quad . \tag{A.16}$$

The difference between the amplitude at 3 in this case and the amplitude at 3 for the previous case is just the quadratic phase factor, indicating a diverging spherical wave component with a 1 focal length radius of curvature. The transmitted field is $u_3^+ = u_3(x_3)\cdot t(x_3)$ where $t(x_3)$ has not changed. Propagating this amplitude a distance f to plane 4 yields

$$u_4(x_4) = \int u_3^+(x_3)\exp(i\pi(x_4 - x_3)^2/\lambda f)dx_3 \quad , \tag{A.17}$$

and multiplying by the transmittance of the lens at 4,

$$u_4^+(x_4) = u_4(x_4)\exp(-i\pi x_4^2/\lambda f)$$

$$= \int u_3^+(x_3)\exp(i\pi((x_4 - x_3)^2 - x_4^2/\lambda f)dx_3$$

$$= \int \tilde{u}_1(x_3/\lambda f)\exp(i\pi x_3^2/\lambda f)$$

$$\cdot \exp(i\pi(-2x_3x_4 + x_3^2)/\lambda f)t(x_3)dx_3 \quad . \qquad (A.18)$$

There is now an additional quadratic phase factor of $\exp(i\pi x_3^2/\lambda f)$ resulting from the longitudinal translation of the input by a distance f. Propagation a distance f beyond plane 4 will no longer be sufficient to obtain an autocorrelation. Note that the first and the fourth terms of $t(x_3)$, the terms which resulted in an image and in an autocorrelation at the output in the first case, still have identical quadratic phase factors. This means that both will focus in the same plane. Therefore, we can find the plane of the autocorrelation by employing geometrical optics to find the image plane. We proceed with the argument. For an afocal system, the longitudinal magnification equals the square of the transverse magnification. The transverse magnification is the negative of the focal length ratio: $m_t = -f_2/f_1$. In a correlator with both lenses of the same focal length, the longitudinal magnification is unity. The correlator with input adjacent to the first lens has had the diffracting object shifted by a distance f. This means that the image of this plane adjacent to the first lens will lie two focal lengths beyond the second lens. Therefore, to find the amplitude at 5, we propagate u_4^+ a distance 2f.

$$u_5(x_5) = \iint \tilde{u}_1(x_3/\lambda f)\exp(i\pi x_3^2/\lambda f)$$
$$\cdot \exp(i\pi(-2x_3x_4 + x_3^2)/\lambda f)t(x_3)$$
$$\cdot \exp(i\pi(x_5 - x_4)^2/2\lambda f)dx_3dx_4 \quad . \tag{A.19}$$

Collecting the terms in x_4,

$$\int \exp(i\pi(-2x_3x_4 - x_4x_5 + x_4^2/2)/\lambda f)dx_4$$
$$= \exp(-i\pi(x_5^2/2 + 2x_5x_3 + 2x_3^2)/\lambda f) \quad . \tag{A.20}$$

Substituting this into the preceding integral for u_5,

$$u_5(x_5) = \int \tilde{u}_1(x_3/\lambda f)t(x_3)\exp(-i2\pi x_3x_5/\lambda f)dx_3 \quad . \tag{A.21}$$

Now we must consider the individual terms in $t(x_3)$ to simplify the expression for u_5. The first term gives rise to an image

$$u_1(-x_5)*\delta(x_5) \quad .$$

The second term is the convolution:

$$u_1(-x_5)*u_1(-x_5)*u_1^*(-x_5)*\delta(x_5) \quad .$$

The third term gives the self-convolution:

$$u_1(-x_5)*u_1(-x_5)*\delta(x_5 + \alpha\lambda f) \quad .$$

And finally, we obtain the autocorrelation:

$$u_1(-x_5) \star u_1(-x_5) * \delta(x_5 - \alpha\lambda f) \quad .$$

We observe that the results are identical to those reached in the first configuration. It was necessary to move the correlator's output plane, as determined by the input's displacement from the first lens's front focal plane. A comparison between the autocorrelation locations is given by Figure A.3. Other than this, the results are identical to the approximation of this treatment. Two sources of higher order errors have been introduced, however. The holographic matched filter was not illuminated in the fashion in which it was constructed. Therefore, we are confronted with holographic aberrations. Secondly, the lenses are used at object and image conjugates different from those of the first case. There will be some change in the lens aberrations resulting from this conjugate shift if the same lens design is used for both applications. Also, vignetting may be encountered in this second case. See Figure A.3(b). In working with a correlator used for fingerprint identification, the author found no measurable changes in the correlator's performance due to these sources.

With the focal lengths identical, the total length is the same as in the first configuration. However, the geometrical optics for the filter maker FTL is different from that for the correlator FTL. It is more economical to make all lenses identical, as they could be for the first configuration.

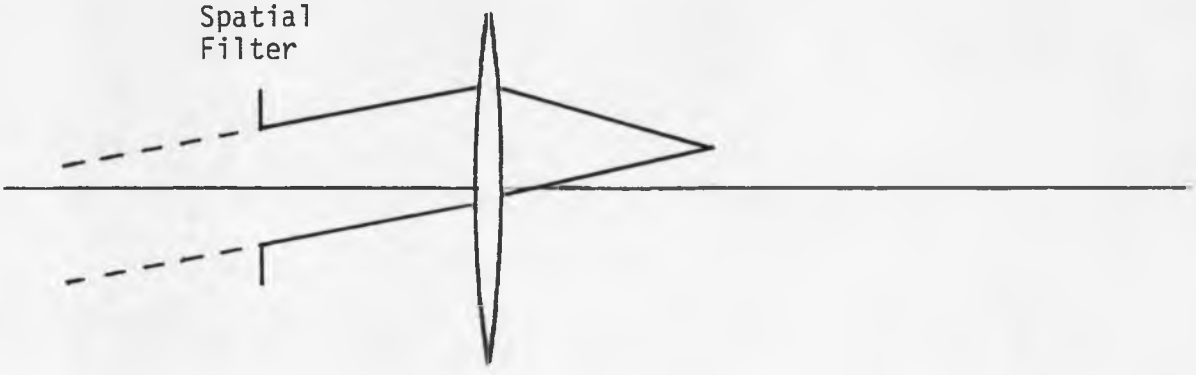

(a) D1 = f

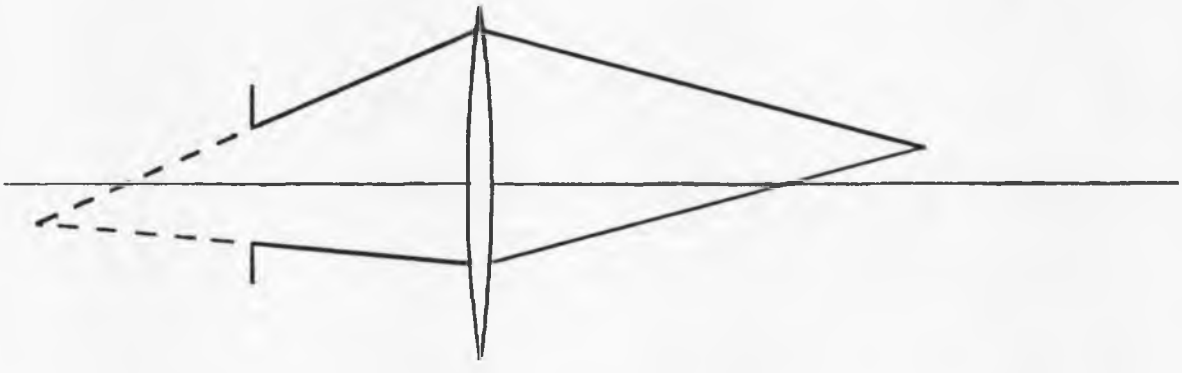

(b) D1 = 0

Figure A.3. Geometrical Optics of Autocorrelation for Two Correlator Configurations.

Filters with a Quadratic Phase Term

To eliminate some of the aberrations in the previous system, the filter could have been made with the transparency in the plane of the lens. The transmittance function for the filter will assume a different form. The amplitude in the rear focal plane of the lens becomes

$$u_3(x_3) = \tilde{u}_1(x_3/\lambda f)\exp(i\pi x_3^2/\lambda f) \quad . \tag{A.22}$$

With the introduction of a coherent plane wave, the recorded irradiance is

$$\begin{aligned} &|\tilde{u}_1(x_3/\lambda f)\exp(i\pi x_3^2/\lambda f) + \exp(i2\pi\alpha x_3)|^2 \\ &\quad = 1 + \tilde{u}_1\tilde{u}_1^* + \tilde{u}_1\exp(i\pi x_3^2/\lambda f)\exp(-i2\pi\alpha x_3) \\ &\qquad + \tilde{u}_1^*\exp(-i\pi x_3^2)\exp(i2\pi\alpha x_3) \quad . \end{aligned} \tag{A.23}$$

With proper processing of the film, this irradiance expression becomes the new expression for the filter's amplitude transmittance $t(x_3)$, neglecting multiplicative constants. (The constants are of interest when calculating irradiance levels for selection of the output plane detector.)

For this last case, assume $x_0 = 0$ for convenience. With the matching signal introduced on axis in the correlator, the field transmitted by the spatial filter is

$$u_3^+(x_3) = u_3(x_3)t(x_3)$$

$$= \tilde{u}_1 \exp(i\pi x_3^2/\lambda f) + \tilde{u}_1\tilde{u}_1\tilde{u}_1^* \exp(i\pi x_3^2/\lambda f)$$

$$+ \tilde{u}_1\tilde{u}_1 \exp(i2\pi x_3^2/\lambda f)\exp(-i2\pi\alpha x_3/\lambda f)$$

$$+ \tilde{u}_1^* u_1 \exp(i2\pi\alpha x_3/\lambda f) \quad . \qquad (A.24)$$

In this case, the first and the second terms in the product will focus in the same plane, but the last two terms will focus in two additional planes, due to the existence of three different quadratic phase factors. The first two terms of $t(x_3)$ having no quadratic phase factors of themselves will focus at the image of the wave leaving the hologram. The phase factor $\exp(i\pi x_3^2/\lambda f)$ appearing in u_3^+ describes a diverging wavefront with center of curvature a distance f to the left of the hologram, or a distance 2f to the left of the second lens. Therefore, it will converge to a point a distance 2f to the right of the second lens, according to the laws of geometrical optics. See Figure A.4(b).

The product of $u_3(x_3)\cdot t(x_3)$ gives the third term of the transmitted field a quadratic phase factor $\exp(i2\pi x_3^2/\lambda f)$. This describes a wavefront with center of curvature f/2 to the left of the hologram, or a distance 3f/2 to the left of the second lens. The light can be considered to be coming from a virtual object 3f/2 to the left of the second lens. Such light focuses a distance 3f to the right of the lens. See Figure A.4(c).

The fourth term of $t(x_3)$ has a quadratic phase factor opposite in sign to that of $u_3(x_3)$ and the product forms a transmitted component

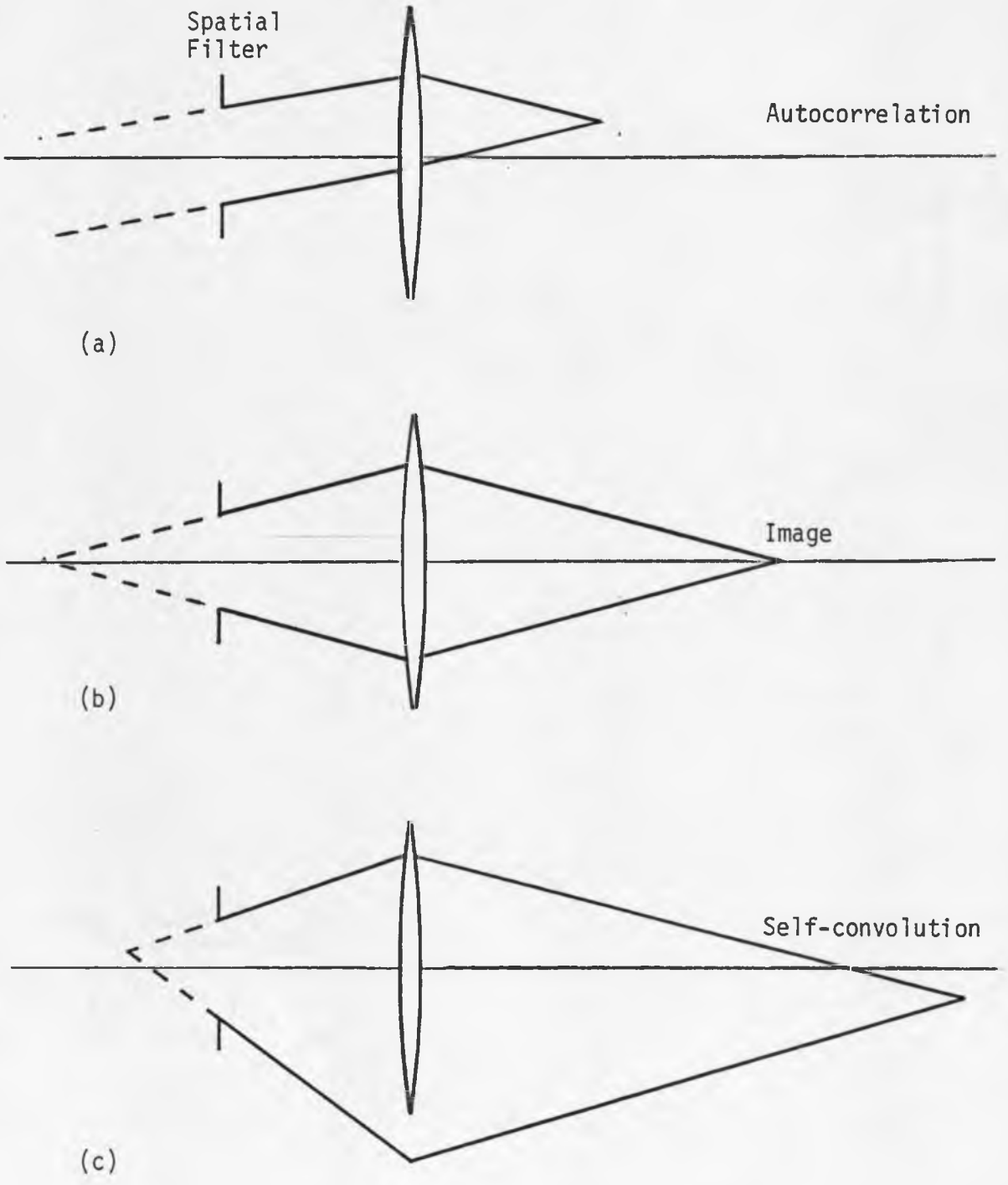

Figure A.4. The Three Focal Planes for a Spatial Filter with Quadratic Phase.

with no quadratic phase, viz., a collimated wave. This component will focus a distance f to the right of the second lens. See Figure A.4(a).

The first two terms focus at heights determined by their convolutions with the distribution $\delta(x_5)$. The third term focuses at height $x_5 = -\alpha\lambda f$. And finally, the autocorrelation lies at $x_5 = \alpha\lambda f$. The figure describes the three foci. The inequalities for separation of the terms become more complicated, but are again straightforward. A larger value for α is now required for separation at the autocorrelation plane because the light forming the self-convolution is still two focal lengths distant from its own focus.

The third system does indeed provide a more compact system than the first. However, the two lenses of the correlator cannot be identical if all aberrations are corrected, for they work at different conjugates, whereas, the first system of filter maker and correlator can be made of three identical lenses. The second system provides us with no advantages and, as in the third system, requires that the lenses work at different conjugate arrangements, necessitating the design and fabrication of more than one lens type for aberration free performance.

Conclusions

In the past several pages, the diffraction theory and the geometrical optics of several examples have been given. There are other configurations of interest (some academic, some practical) such as a spherical reference wave, transparency behind the lens, second lens adjacent to the spatial filter, etc. Though these are not treated here, the methods for examining their feasibility and the properties of the

feasible configurations have been presented with examples. Two concepts of particular usefulness were Cathey's (1974, p. 372) formulation for Fourier transforming quadratic phase factors and the use of geometrical optics for determining distances. It is far easier to calculate distances to foci from knowledge of the centers of curvature of wavefronts than from examination of the lengthy quadratic phase terms, incorporating D1 and D2 as variables in the diffraction integrals. It is shown in these three examples that a combination of scalar wave theory and geometrical optics methods allows for ready determination of system properties. Fresnel-Kirchhoff integrals are not so cumbersome if they are supplemented by good Fourier transform formulas and a knowledge of paraxial optics.

The unequal focal length system given in Table 3.2 was not treated in this appendix, but the only key difference is that the Fourier transform variable for the calculations changes from $x_i/\lambda f_1$ to $x_i/\lambda f_2$ when passing to the second lens. This merely scales the terms at the output by the lateral magnification of the afocal system: $m_t = -f_2/f_1$. This type of arrangement produces a more compact correlator, at the expense of raising the numerical aperture of the second lens when the focal length is decreased.

There are several advantages to using the spacing selection $f_1 - f_1 - f_2 - f_2$ in the correlator. At least two of the lenses, the filter maker lens and the correlator FTL, can be made identical and aberration free simultaneously. The information carrying light stays reasonably close to the axis (when a prism and plate assembly are

introduced), so that an unusually large aperture is not required of the second lens. The light forming the autocorrelation is collimated leaving the matched filter, so the prism and plate do not introduce any aberrations (other than a small amount of anamorphic distortion for beams not falling upon the prism at the angle of minimum deviation). Aberrations introduced by the prism cannot be corrected by a rotationally symmetric optical system, so they should be avoided. The spatial filter made with the f - f spacing contains no quadratic phase factor, making it a lesser source of the holographic aberrations introduced when the matching input is introduced to the correlator off axis. Also, the $f_1 - f_1 - f_2 - f_2$ spacing is the only arrangement for which the psf of the filter maker and for the correlator can be ideally isoplanatic. The other configurations may result in all chief rays being nearly orthogonal to plane 5, but it is obvious that only the doubly telecentric aberration free system is mathematically isoplanatic.

APPENDIX B

CARD IMAGES FOR DESIGN OF A FOURIER TRANSFORM LENS

Problems were experienced in the optimization of telecentric systems. Some programs trace real rays from the last glass surface to the exit pupil and then to the focal surface. When the distance to the exit pupil is very large, as in the design of a Fourier transform lens, the calculations give erroneous results due to the lack of word length in the computer. For instance, it was necessary to write the input deck in the form given in Appendix C in order to optimize the 235 mm efl triplet Fourier transform lens used in the unequal focal lengths correlator described in Table 3.2. Not all programs will have this difficulty.

In the list of card images given below, "TH" refers to the axial thickness following the surface, the "GLASS" entry is the index of refraction following the surface, and "RD" gives the radius of curvature of the surface. A "GLASS" or "AIR" card signals the end of information for a particular surface. All card images are in uppercase letters.

ACCOS II Input Deck for the Design of a Fourier Transform Lens

Card Images	Legend
LENS	Start of input deck.
FT LENS	Title card.
PARAXBUCH -.019E10 18	Paraxial chief ray height at object and entrance pupil radius.

Card Images		Legend
TH	1E10	Thickness to next surface.
AIR		End of data for surface 0, the object.
AIR		End of data for surface 1, the entrance pupil.
TH	191.	Thickness to first glass surface.
VARY TH		
AIR		End of data for surface 2.
RD	124.	
TH	10.	
VARY CV		
GLASS	1.77866	End of data for surface 3.
RD	-923.	
TH	25.	
VARY CV		
VARY TH		
AIR		End of data for surface 4.
RD	-141.4	
TH	10.	
VARY CV		
PIKUPGLASS	3	Refractive index following surface 5 is to be same as that following surface 3.
PIKUPCVM	5	Curvature of this surface is to be negative of the curvature of surface 5.
PIKUPTH	4	
AIR		End of data for surface 6.

Card Images	Legend
PIKUPCVM 4	
PIKUPTH 3	
PIKUPGLASS3	End of data for surface 7.
PIKUPCVM 3	
PIKUPTH 2	
AIR	End of data for surface 8.
AIR	End of surface 9.

The "PIKUPTH 2" instruction makes the back focal distance the same as the stop to first element thickness. Thus, symmetry is enforced even while the back focal distance is variable. (In the usual thin lens description of the Fourier transform properties, the focal length of the lens, its front focal distance and its back focal distance are identical. However, the requirement that the transparency be in the front focal plane means precisely that; it does not mean that the transparency be one focal length from the lens, but that it be one focal length from the first principal plane of the lens.)

The rays represented in Figure B.1 were used to define a defect function to be minimized by the program. For ACCOS II, the card images are these:

Card Images	Legend
ACCOS	
RAY 1 0 0 .7	Axial rays.
RAY 2 0 0 .95	

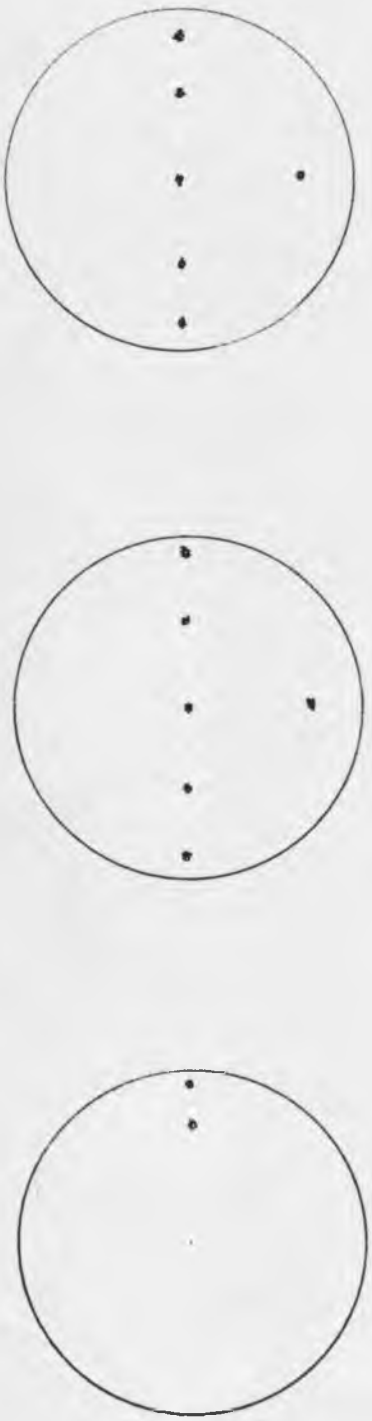

Figure B.1. Entrance Pupil Intersections of Rays Traced to Define the Defect Function.

Card Images				Legend	
RAY	3	.7	0 .9		
RAY	4	.7	0 .5		
RAY	5	.7		70% field chief ray	70% field rays.
RAY	6	.7	0 -.5		
RAY	7	.7	0 -.9		
RAY	8	.7	.7	Sagittal ray	
RAY	9	1	0 .8		
RAY	10	1	0 .5		
RAY	11	1	0	Full field chief ray	Full field rays.
RAY	12	1	0 -.5		
RAY	13	1	0 -.85		
RAY	14	1	.7	Sagittal ray	

The terms in the defect functions are the squared differences between the intercept of each nonchief ray and the intercept of the chief ray for the respective field positions. Thus, there are twelve defect terms defined for this set of rays. In card image form they are:

Card Images					
SA1	YK	1			
SA2	YK	2			
DY1	YK	3	5	1	1
DY2	YK	4	5	1	1
DY3	YK	6	5	1	1
DY4	YK	7	5	1	1

Card Images

```
DX1  XK   8
DY5  YK   9  11 1 1
DY6  YK   10 11 1 1
DY7  YK   12 11 1 1
DY8  YK   13 11 1 1
DX2  XK   14
PWR  POWER
```

The pairs of "1's" are weights assigned to the values of the ray heights. For example, DY4 is the difference between the y coordinate of ray number 7 and the y coordinate of ray number 5 at the image surface.

The program is instructed to optimize the lens according with these instructions:

Card Images	Legend
MINZ SA1	
MINZ SA2	
MINZ DY1	
MINZ DY2	
MINZ DY3	
MINZ DY3	
MINZ DY4	
MINZ DY5	
MINZ DY6	

Card Images	Legend
MINZ DY7	
MINZ DY8	
MINZ DX1	
MINZ DX2	
MINZ PWR .004267 100	This request for focal length is not used when the best focus of a designed lens is being sought, especially when the best focal plane of an afocal system is being determined.

Thus, the quadratic form to be minimized is

$$(SA1)^2 + (SA2)^2 + \sum_{N=1}^{8} (DYN)^2 + (DX1)^2 + (DX2)^2 + ((POWER - .004267)\cdot 100)^2.$$

Note that no distortion terms appear in the defect function. The lens is considered perfect with respect to this defect function if (1) it has power .004267, (2) the rays from one object point meet at a point in image space, and (3) the image points for the several object points lie in a plane orthogonal to the optical axis.

APPENDIX C

CARD IMAGES FOR EVALUATION OF LENSES

Evaluation of a Fourier Transform Lens

This section contains an annotated description of the card images used in an ACCOS V run for the calculation of ray fans and psf's for a FTL. All the card images are in uppercase letters.

Card Images	Legend
LENS	
LI, CEMENTED APLANAT	
SAY, 18	Input aperture height above the optical axis is 18 mm.
WV, .6328 .6328 .6328	
SCY, -.019E10	The paraxial field height is 1.9×10^8 mm.
TH, 1E10	The distance to the next surface is 10^{10} mm.
AIR	End of data for object surface.
AIR	Dummy surface representing entrance pupil. Chief rays pass through the axis at this surface, but no search for the exit pupil is implemented.
AIR	
RD, 173.6676	
TH, 9.4	
SCHOTT SK5	
RD, -83.0344	

Card Images	Legend
TH, 2.35	
SCHOTT SF12	
RD, -405.2721	
TH, 229.19885	
AIR	
EOS	End of lens description subfile.
LEPRT	The lens description is printed, along with pertinent first order properties.
MACRO FTEVAL	A user written internal subroutine, or MACRO, called FTEVAL is constructed. It ends with the card image EOM. Such a subroutine can be introduced bodily at execution time by using the MACRO's title as a card image.
FOB	Fans of rays are traced from an axial point, from a .7 full field point, and from a full field point.
RAY	
PRXYD ALL	
YFAN OPD,0 1 1 11	
FOB,.7	
RAY	
PRXYD ALL	
YFAN OPD,-1 1 1 21	
XFAN OPD,0 1 1 11	
FOB,1	
RAY	
PRXYD ALL	

Card Images	Legend
YFAN OPD,-1 1 1 21	
XFAN OPD,0 1 1 11	
FOB	
DEP	Enter the diffraction subroutines of ACCOS V for the calculation of wavefront variances and point spread functions.
VAR	
M, IRRADIANCE SCALED TO UNITY AT ORIGIN	
M, FOR AN ABERRATION FREE WAVEFRONT	
	The messages following the commas are printed each time the subroutine is called.
C, BEFORE EXECUTING THE MACRO, EDIT THE NEXT INSTRUCTION	
C, AND ITS FOB,.7 and FOB,1 COUNTERPARTS	
C, SO THAT THE PSF IS PROPERLY SAMPLED	
	Internal comments used as a reminder that instructions for psf calculations need to be modified in consideration of the lens's numerical aperture.
PTSP S,0 .015 .0015	Calculate the values of the axial psf along a sagittal section from the optical axis to .015 mm from the axis in .0015 mm increments.
EOS	
FOB,.7	
DEP	
VAR	
PTSP S,0 .015 .0015	

Card Images	Legend
PTSP T,-.015 .015 .0015	Calculate values of the psf along a tangential section from .015 mm below the .7 field chief ray intercept with the focal surface to .015 mm above it in .0015 mm increments.
EOS	
FOB,1	
DEP	
VAR	
PTSP S,0 .015 .0015	
PTSP T,-.015 .015 .0015	
EOS	
EOM	The subroutine is now stored internal to ACCOS V and may be called into use simply by using its name as a command.
FTEVAL	ACCOS V executes the instructions contained in the subroutine on the lens currently in the active lens storage area.

Evaluation of the Afocal Doubly Telecentric Imaging Configuration

Card Images	Legend
LENS	
LI, CEMENTED APLANATS IN THE IMAGING CONFIGURATION	
WV, .6328 .6328 .6328	
SAY, 4.5	Paraxial marginal ray height on first surface.
SCY, -18	Edge of the input format.
TH, 233.1595	
RD, 173.6676	
TH, 9.4	
SCHOTT SK5	
RD, -83.0344	
TH, 2.35	
SCHOTT SF12	
RD, -405.2721	
TH, 229.199	
AIR	
TH, 229.199	
REFS	The paraxial chief ray will not pass through the center of the holographic filter. To insure that the real chief ray does, the reference surface instruction is added here. To insure that the real marginal ray passes through the edge of the hologram, the clear aperture specification is given: $235 \cdot \sin\theta = 4.5$. In the case of some older programs, the specification of the surface as the aperture was necessary to get the paraxial chief ray through this point. Then

Card Images	Legend
	there arose the difficulty of getting the marginal ray through the edge of the hologram. Even more trying was specifying off axis ray fans in the imaging configuration. The difficulty was not insurmountable, for I once worked out a method to design and analyze lenses on such programs. However, the capabilities of ACCOS V enable the designer to perform this task in a fairly straightforward manner.
	The use of a REFS instruction implements a ray search scheme to send the chief ray through the optical axis at the reference surface, but without causing a search for the infinitely distant entrance and exit pupils.
CLAP, 4.5	
AIR	
RD, 405.2721	
TH, 2.35	
SCHOTT SF12	
RD, 83.0344	
TH, 9.4	
SCHOTT SK5	
RD, -173.6676	
TH, 231.472433	
AIR	
EOS	
FTEVAL	The instructions in MACRO FTEVAL are now executed.

APPENDIX D

CARD IMAGES FOR OPTIMIZATION OF A FOURIER TRANSFORM LENS AT TWO WAVELENGTHS

Lens Description

For the optimization of the Fourier transform lens at two wavelengths, the multiple configuration option of ACCOS V was used.

Card Images	Legend
LENS	
LI, MULTIPLE WAVELENGTH FOURIER TRANSFORM LENS	
SAY, 20	
SCY, -.04E10	
WV, .6328 .488 .5876	
TH, 1E10	
AIR	
AIR	Surface 1 coincides with surface 2 and is the reference surface and entrance pupil.
TH, 431	
AIR	
RD, 240	
TH, 12.5	
SCHOTT BAK1	
RD, -908	
TH, 48	

Card Images	Legend
AIR	
RD, -240	
TH, 8	
SCHOTT BK7	
PIKUP CV, 5 -1	
PIKUP TH, 4	
AIR	
PIKUP CV, 4 -1	
PIKUP TH, 3	
PIKUP GLASS, 3	
PIKUP CV, 3 -1	
PIKUP TH, 2	
AIR	
EOS	
CONFIGS	
CFG, 2	
TH, 2 421.15	
EOS	

Defect Function

For optimization of the lens, a set of commands stored internally to ACCOS V was created.

The explanation of this defect function can be understood with the aid of an ACCOS V User's Manual (Scientific Calculations, Inc.,

1976). The only comment here will be a short explanation of the implementation of the defects in the second color.

Ray 2 is an axial zonal ray traced at the second wavelength. Defects involving rays traced in the control wavelength, wavelength 1, such as DY3 are defined by the single symbol DY, which the program reads as the difference between the y intercept of ray 3 and the y intercept of the chief ray from the same field point. However, in order to define the similar defect at the second wavelength, it is necessary to explicitly define a chief ray at wavelength 2, viz., RAY 8. Then the counterpart of DY3, DY7 is defined as the difference between the y value of ray 8 and the y value of ray 9 (see lines 49 through 51).

This means of defining the defects is not explicitly covered in the ACCOS V Manual at the time of this writing, but was deduced from the response of the program to other attempts to implement the multiwavelength defect function. The following is a listing of the card images for the multiwavelength defect function called FTTWOL.

Card Images:

```
 1.  MACRO FTTWOL
 2.  RAYSET
 3.  FOB
 4.  RAY 1,.7
 5.  RAY 2,.7 0 2
 6.  FOB,.7
 7.  RAY 3,.85
 8.  RAY 4,.55
 9.  RAY 5,-.55
10.  RAY 6,-.85
11.  RAY 7,0 .7
12.  RAY 8,0 0 2
13.  RAY 9,.85 0 2
14.  RAY 10,.55 0 2
15.  RAY 11,-.55 0 2
```

Card Images, Continued:

```
16.  RAY 12,-.85 0 2
17.  RAY 13,0 .7 2
18.  FOB,1
19.  RAY 14,.85
20.  RAY 15,.55
21.  RAY 16,-.55
22.  RAY 17,-.85
23.  RAY 18,0 .7
24.  RAY 19,0 0 2
25.  RAY 20,.85 0 2
26.  RAY 21,.55 0 2
27.  RAY 22,-.55 0 2
28.  RAY 23,-.85 0 2
29.  RAY 24,0 .7 2
30.  EOS
31.  DEFINITIONS
32.  Y8 Y,8
33.  Y9 Y,9
34.  Y10 Y,10
35.  Y11 Y,11
36.  Y12 Y,12
37.  Y19 Y,19
38.  Y20 Y,20
39.  Y21 Y,21
40.  Y22 Y,22
41.  Y23 Y,23
42.  DY1 DY,1
43.  DY2 DY,2
44.  DY3 DY,3
45.  DY4 DY,4
46.  DY5 DY,5
47.  DY6 DY,6
48.  DX1 X,7
49.  COM DY7
50.  ADD Y8
51.  ADD Y9,-1
52.  COM DY8
53.  ADD Y8
54.  ADD Y10,-1
55.  COM DY9
56.  ADD Y8
57.  ADD Y11,-1
58.  COM DY10
59.  ADD Y8
60.  ADD Y12,-1
61.  DX2 X,13
62.  DY11 DY,14
63.  DY12 DY,15
```

Card Images, Continued:

```
64.  DY13 DY,16
65.  DY14 DY,17
66.  DX3 X,18
67.  COM DY15
68.  ADD Y19
69.  ADD Y20,-1
70.  COM DY16
71.  ADD Y19
72.  ADD Y21,-1
73.  COM DY17
74.  ADD Y19
75.  ADD Y22,-1
76.  COM DY18
77.  ADD Y19
78.  ADD Y23,-1
79.  DX4 X,24
80.  PWR PWRY,2 9
81.  EOS
82.  REQUESTS
83.  CFG,1
84.  DY1
85.  DY3
86.  DY4
87.  DY5
88.  DY6
89.  DX1
90.  DY11
91.  DY12
92.  DY13
93.  DY14
94.  DX3
95.  PWR,.002 200
96.  CFG,2
97.  DY2
98.  DY7
99.  DY8
100. DY9
101. DY10
102. DX2
103. DY15
104. DY16
105. DY17
106. DY18
107. DX4
108. EOS
109. VARIABLES
110. GLOBAL
111. CV,3
```

Card Images, Continued:

```
112.  CV,4
113.  CV,5
114.  TH,4
115.  CFG,1
116.  TH,2
117.  CFG,2
118.  TH,2
119.  EOS
120.  EOM
EOF
```

Such a lens is now easily evaluated by (1) successively updating the lens in storage to make each wavelength the control wavelength, (2) calling for the proper "CONFIGS" data for the lens, and then (3) executing FTEVAL (see Appendix C).

REFERENCES

ACCOS V User's Manual, Scientific Calculations, Inc., 1976, Rochester, New York.

Blandford, B. A. F., 1970, Optical Instruments and Techniques, pp. 436-443. Ed. J. H. Dickson, Oriel Press, Newcastle upon Tyne.

Born, Max, and Emil Wolf, 1959, Principles of Optics, 1st Edition, Pergamon Press, New York.

Cathey, Wade Thomas, Jr., 1974, Optical Information Processing and Holography, Wiley-Interscience, New York.

Fienup, J. R., 1977, "Analysis of Holographic Optics for Optical Processors," Interim Scientific Report for Contract FF44620-76-C-0047 for Directorate of Electronics and Solid State Sciences, AFOSR/NR, Building 410, Bolling AFB, Washington, D.C. 20332.

Goodman, Joseph W., 1968, Introduction to Fourier Optics, McGraw-Hill, New York.

Matsui, Y., S. Minami, and S. Yamaguchi, 1974, "Aberration Theory Applied to Design of Fourier Transform Lens System" (in Japanese, translated by Peter Adachi of Minolta Corporation) Optics Division, Canon, Inc., Tokyo.

Steel, W. H., 1973, "A Simple Lens for Optical Fourier Transforms," Optics Communications 2(2):36-37.

von Bieren, K., 1971, "Lens Design for Optical Fourier Transform Systems," Applied Optics 10(12):2739-2742.

Wynne, C. G., 1974a, "Simple Fourier Transform Lenses-I," Optics Communications 12(3):266-269.

Wynne, C. G., 1974b, "Simple Fourier Transform Lenses-II," Optics Communications 12(3):270-274.